

## Post-canard symmetry breaking and other exotic dynamic behaviors in identical coupled chemical oscillators

Naziru M. Awal and Irving R. Epstein<sup>✉</sup>

Department of Chemistry, MS 015, Brandeis University, Waltham, Massachusetts 02453, USA



(Received 20 December 2019; revised manuscript received 3 March 2020; accepted 7 April 2020; published 30 April 2020)

We analyze a model of two identical chemical oscillators coupled through diffusion of the slow variable. As a parameter is varied, a single oscillator undergoes a canard explosion—a transition from small amplitude, nearly harmonic oscillations to large-amplitude, relaxation oscillations over a very small parameter interval. In the coupled system, if the two oscillators have the same initial conditions, then the oscillators remain synchronized and exhibit the same canard behavior observed for the single oscillator. If the oscillators are separated initially, then in the region of the canard they display a variety of complex behaviors, including intermittent spiking, mixed-mode oscillation, and quasiperiodicity. Further variation of the parameter leads to a return to synchronized large-amplitude oscillation followed by a post-canard symmetry-breaking, in which one oscillator shows small-amplitude, complex behavior (mixed-mode oscillation, quasiperiodicity, chaos,...) while the other undergoes essentially periodic large amplitude behavior, resembling a master-slave scenario. We analyze the origins of this behavior by looking at several modified coupling schemes.

DOI: [10.1103/PhysRevE.101.042222](https://doi.org/10.1103/PhysRevE.101.042222)

### I. INTRODUCTION

Many systems in biology, chemistry, and physics consist of coupled oscillators, a phenomenon that has interested scientists at least as far back as Huygens' 17th-century studies of pendulum clocks hanging on a common wall [1]. In recent years, there have been a number of studies, many inspired by the behavior of coupled neurons [2–7], on oscillators in which variables evolve on very different (“slow” and “fast”) timescales, resulting in *relaxation oscillations*, in which the limit cycle consists of a slow buildup followed by a sudden discharge [8,9]. One scenario in which relaxation oscillations can emerge as a parameter is varied in a single nonlinear oscillator with multiple timescales is via a *canard explosion* [10–12]. In a range of parameter values, the system possesses only a stable fixed point. As a parameter is increased (or decreased), the system passes through a Hopf bifurcation, where the fixed point loses stability and small amplitude, nearly harmonic oscillations begin. At a somewhat higher parameter value, the canard explosion occurs. The oscillations increase sharply in amplitude, typically by an order of magnitude or more, over a narrow range of the parameter and take on the anharmonic waveform of a relaxation oscillator. The canard explosion is sometimes accompanied by more complex dynamical behavior, notably *mixed-mode oscillations* (MMOs), in which each cycle of oscillation consists of one or more large amplitude spikes and one or more small amplitude peaks. Mixed-mode behavior associated with multiple timescales has been analyzed in detail by Desroches *et al.* [13–18]. In systems of coupled relaxation oscillators, *localized behavior* can

arise, characterized by clusters of oscillators [19,20], in which the oscillators in each cluster display the same amplitude and period, but the clusters differ from one another in amplitude, period, and/or phase.

With large numbers (dozens to hundreds) of coupled nonlinear oscillators, a novel phenomenon, a *chimera*, may occur, in which one subset of oscillators behaves in a coherent, synchronized fashion, while the remainder oscillate incoherently [21–28]. Recently, there has been interest in the possibility of chimeric behavior in small, perhaps minimal, arrays of coupled oscillators. Kapitaniak *et al.* [29,30] reported chimeralike behavior in three-oscillator systems, and we recently suggested that two identical diffusively coupled Lengyel-Epstein (LE) oscillators [31], in which one shows large-amplitude relaxation oscillations, while the other exhibits small amplitude chaos, constitute the smallest possible example of a chimeric system. In this paper, we examine that system further and discover that, in addition to the chimeric behavior, it displays a remarkable variety of exotic dynamical behavior as a control parameter is varied, including a phenomenon that we dub post-canard symmetry-breaking (PCSB), which occurs after the multiple behaviors induced by the canard explosion have reverted to in-phase synchrony.

This work is organized as follows. In Sec. II, we examine the uncoupled system and introduce the canard phenomenon. In Sec. III, we consider the diffusively coupled (DC) system, which consists of two identical LE oscillators coupled via diffusion of the slow inhibitor species. We analyze the canard critical point for the coupled system. To gain insight into our results, we introduce modified coupling schemes, illustrated schematically in Fig. 1, in which only the autonomous (self-disinhibition) or the nonautonomous (cross-coupling) terms are retained, as well as a “master-slave” scenario, in

<sup>✉</sup>epstein@brandeis.edu

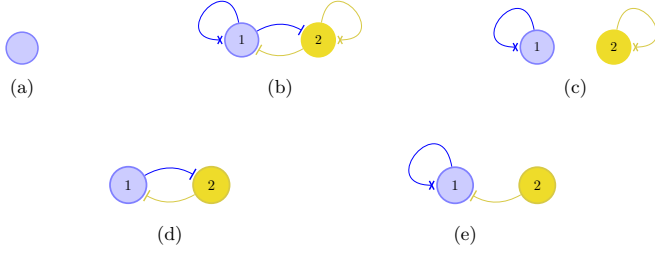


FIG. 1. Representation of different coupling schemes. (a) Uncoupled. (b) Diffusively coupled. (c) Self-disinhibition. (d) Cross-coupling. (e) Master-slave.

which the coupling is unidirectional. In Sec. IV, we compare the coupling schemes, varying several parameters. We seek to understand the origin of the multiple modes of complex behavior observed, particularly the PCSB. We conclude by summarizing our results and suggesting possible future directions.

## II. THE UNCOUPLED SYSTEM

The Lengyel-Epstein (LE) model describes temporal oscillations and Turing (spatial) patterns in the chlorine dioxide-iodine-malonic acid (CDIMA) [32] and chlorite-iodide-malonic acid (CIMA) [33] reactions. In its simplest form, it consists of two ordinary differential equations that characterize the rates of change of the activator and inhibitor concentrations. The equations for its time evolution are

$$\begin{aligned} \frac{du}{dt} &= a - u - \frac{4uv}{1+u^2}, \\ \frac{dv}{dt} &= \sigma b \left( u - \frac{uv}{1+u^2} \right), \end{aligned} \quad (1)$$

where  $u$  is the dimensionless concentration of the activator, which corresponds to the iodine-containing species, and  $v$  is the dimensionless concentration of the inhibitor, which corresponds to the chlorine-containing species. Both  $a$  and  $b$  are parameters related to the feed concentrations, and  $\sigma$  represents the degree of complexation of the activator with an immobile indicator. Under typical laboratory conditions, the parameters lie in the range  $0 < a < 35$ ,  $0 < b < 8$  and  $1 < \sigma < 8$  [33,34]. Here we consider the case  $\sigma b = \beta \ll 1$ .

### A. Change of variables

It is convenient to eliminate the nonlinearity in the second equation in Eq. (1), thereby ensuring that one nullcline is linear. To do this, we set  $\beta = \sigma b$  and introduce a new variable,  $w$ :

$$\begin{aligned} w &= -\beta u + 4v, \\ v &= \frac{\beta u + w}{4}. \end{aligned} \quad (2)$$

The equations in the new variables become

$$\frac{du}{dt} = a - u - \frac{u(\beta u + w)}{1+u^2}, \quad \frac{dw}{dt} = -\beta(a - 5u). \quad (3)$$

In these new variables, the  $u$  and  $w$ -nullclines are, respectively,

$$\begin{aligned} w &= \frac{(a-u)(1+u^2) - u^2\beta}{u} \equiv f_1(u, \beta), \\ u &= \frac{a}{5}. \end{aligned} \quad (4)$$

Let  $(u_m, w_m)$  be the minimum of the cubic-like  $u$ -nullcline, given by

$$0 = 2u_m^3 + (\beta - a)u_m^2 + a \quad (5)$$

and

$$\begin{aligned} w_m &= \frac{(a-u_m)(1+u_m^2) - \beta u_m^2}{u_m} \\ &= \frac{u_m^3 - u_m + 2a}{u_m}. \end{aligned} \quad (6)$$

Equation (3) has a unique fixed point at

$$(u^*, w^*) = \left( \frac{a}{5}, \frac{4a^2 - 5a\beta + 100}{25} \right), \quad (7)$$

with Jacobian

$$J^* = \begin{bmatrix} \frac{3a^2 - 5a\beta - 125}{a^2 + 25} & -\frac{5a}{a^2 + 25} \\ 5\beta & 0 \end{bmatrix}, \quad (8)$$

trace

$$\text{Tr}(J^*) = \frac{3a^2 - 5a\beta - 125}{a^2 + 25}, \quad (9)$$

and determinant

$$\Delta(J^*) = \frac{25a\beta}{a^2 + 25}. \quad (10)$$

Since the determinant is always positive, a Hopf bifurcation occurs when  $\text{Tr}(J^*) = 0$  (and  $a > 0$ ), i.e., at

$$a_H = \frac{5}{6}(\beta + \sqrt{60 + \beta^2}). \quad (11)$$

Solving Eq. (11) for  $\beta$  in terms of  $a_H$  gives

$$\beta = \frac{3a_H^2 - 125}{5a_H}. \quad (12)$$

### B. Finding the critical points

We employ the approach of Krupa and Szmolyan [35] for finding the canard critical point of a slow-fast system in which the nullcline for the fast variable, in our case  $u$ , since we take  $\beta \ll 1$ , has a cubic-like minimum. We define  $\lambda$ , the distance in  $u$  between the steady state and the minimum of the  $u$ -nullcline, as

$$\lambda = \frac{a}{5} - u_m. \quad (13)$$

We rewrite Eq. (3) using Eqs. (4) and (13):

$$\begin{aligned} \frac{du}{dt} &= [f_1(u, \beta) - w] \frac{u}{1+u^2} \equiv [f_1(u, \beta) - w]f_2(u) \\ &\equiv F(u, w), \end{aligned}$$

$$\begin{aligned} \frac{dw}{dt} &= -5\beta(\lambda + u_m - u) = \beta(5u - 5\lambda - 5u_m) \\ &\equiv \beta G(u, w, \lambda). \end{aligned} \quad (14)$$

We then put Eq. (14) into canonical form [35] (see Appendix A),

$$\begin{aligned} \frac{dx}{d\tau} &= -yh_1(x, y, \lambda, \beta) + x^2h_2(x, y, \lambda, \beta) + \beta h_3(x, y, \lambda, \beta), \\ \frac{dy}{d\tau} &= \beta[xh_4(x, y, \lambda, \beta) - \lambda h_5(x, y, \lambda, \beta) + yh_6(x, y, \lambda, \beta)], \end{aligned} \quad (15)$$

where

$$\begin{aligned} h_3(x, y, \lambda, \beta) &= \mathcal{O}(x, y, \lambda, \beta), \\ h_j(x, y, \lambda, \beta) &= 1 + \mathcal{O}(x, y, \lambda, \beta), \quad (16) \\ j &= 1, 2, 4, 5. \end{aligned}$$

Following Krupa and Szmolyan [35], we set

$$\begin{aligned} a_1 &= \bar{h}_{3x} = \frac{d}{dx}(\bar{f}_2 \bar{f}_3 \beta) = \frac{d}{dx} \left[ -\frac{(5u_m^9)^{1/2}}{(1+u_m^2)^{1/2}a - u_m^3} \right] \\ &= 0, \\ a_2 &= \bar{h}_{1x} = -\frac{5u_m^2(u_m^2 - 1)}{(a - u_m^3)[5u_m(1 + u_m^2)]^{1/2}}, \\ a_3 &= \bar{h}_{2x} = -\frac{5u_m^2(2au_m^2 - u_m^5 + u_m^3)}{(a - u_m^3)^2[5u_m(1 + u_m^2)]^{1/2}}, \\ a_4 &= \bar{h}_{4x} = 0, \\ a_5 &= \bar{h}_6 = 0, \end{aligned} \quad (17)$$

where the overbar notation signifies that the quantities are evaluated at  $(u_m, w_m)$ .

If we consider  $\lambda$  to be the control parameter, then the Hopf critical point is given by [35]

$$\lambda_H(\sqrt{\beta}) = -\left(\frac{a_1 + a_5}{2L_H}\right)\beta + \mathcal{O}(\beta^{3/2}), \quad (18)$$

and the canard critical point is given by

$$\lambda_c(\sqrt{\beta}) = -\left(\frac{a_1 + a_5}{2L_c} + \frac{A}{8L_c}\right)\beta + \mathcal{O}(\beta^{3/2}), \quad (19)$$

where

$$A = -a_2 + 3a_3 - 2a_4 - 2a_5 \quad (20)$$

and

$$L_q = \frac{a_q - u_{m_q}^3}{[5u_{m_q}^5(1 + u_{m_q}^2)]^{1/2}}, \quad (21)$$

with  $q = H$  (Hopf) or  $c$  (canard). Since  $a_1 = a_5 = 0$ , the predicted Hopf critical point from Eq. (18) is  $\lambda_H = 0$ .

Substituting  $u_m$  in terms of  $\lambda_H$  and  $a_H$  from Eq. (13) and  $\beta$  in terms of  $a_H$  from Eq. (12) into Eq. (5) yields an equation for  $\lambda_H$  that clearly has a root at  $\lambda_H = 0$ . In other words, the Hopf critical value from the linear stability analysis is in agreement with that obtained from the Krupa-Szmolyan (KS) analysis.

TABLE I. Hopf and canard critical points of the uncoupled system from linear stability analysis, numerical simulation, and KS analysis

$\beta$	$a_H$ LSA	$u_{m_H}$	$a_c$ sim	$u_{m_c}$	$\lambda_c$ sim	$\lambda_c$ KS
0.001	6.45581	1.29116	6.46001	1.29074	$1.26 \times 10^{-3}$	$1.31 \times 10^{-3}$
0.003	6.45747	1.29150	6.47033	1.29021	$3.85 \times 10^{-3}$	$3.88 \times 10^{-3}$
0.005	6.45914	1.29183	6.48110	1.28964	$6.58 \times 10^{-3}$	$6.40 \times 10^{-3}$

In Table I we summarize  $a_H$  and  $u_{m_H}$  for the Hopf critical points at several values of  $\beta$  as well as the  $a_c$ ,  $u_{m_c}$ , and  $\lambda_c$  obtained from numerical simulations. Comparison of the simulated and analytic canard critical points shows that the KS approximation, which should be exact at  $\beta = 0$ , is quite good at these values of  $\beta$ .

### III. THE DIFFUSIVELY COUPLED SYSTEM

We found in our earlier study [31] that coupling through the activator,  $u$ , has only a minor effect on the dynamical behavior of the system, so we focus here on coupling through the inhibitor,  $v$ . The original Lengyel-Epstein model coupled diffusively through the inhibitor variable is

$$\begin{aligned} \frac{du_i}{dt} &= a - u_i - \frac{4u_i v_i}{1 + u_i^2}, \\ \frac{dv_i}{dt} &= \beta \left[ u_i - \frac{u_i v_i}{1 + u_i^2} + D_v(v_j - v_i) \right], \\ i &= 1, 2; j = 3 - i. \end{aligned} \quad (22)$$

With the change of variables from Eq. (2), Eq. (22) becomes

$$\begin{aligned} \frac{du_i}{dt} &= a - u_i - \frac{u_i(u_i\beta + w_i)}{1 + u_i^2}, \\ \frac{dw_i}{dt} &= \beta[5u_i - a + D_v(\beta(u_j - u_i) + w_j - w_i)], \\ i &= 1, 2; j = 3 - i. \end{aligned} \quad (23)$$

We let

$$\begin{aligned} \Delta a_H &= a - a_H, \\ \Delta a_c &= a - a_c, \end{aligned} \quad (24)$$

where  $\Delta a_H < 0$  and  $\Delta a_H > 0$  represent pre-Hopf and post-Hopf bifurcation and  $\Delta a_c < 0$  and  $\Delta a_c > 0$  represent pre-canard and post-canard, respectively.

#### A. Numerical simulations

We carry out numerical simulations of the diffusively coupled system with  $D_v = 0.1552$  over a range of  $a$  for several values of  $\beta$ . Figure 2 shows a two-parameter bifurcation diagram varying  $a$  and  $\beta$ . Each of the  $\beta$ 's studied exhibits similar patterns. For the sake of simplicity we present, for the most part, results with  $\beta = 0.001$ . When the two oscillators begin with identical initial conditions, the dynamics is, as expected, the same as that observed for the single uncoupled oscillator, with steady state (SS) behavior at  $\Delta a_H < 0$  evolving into synchronized small amplitude oscillations (SAO) via

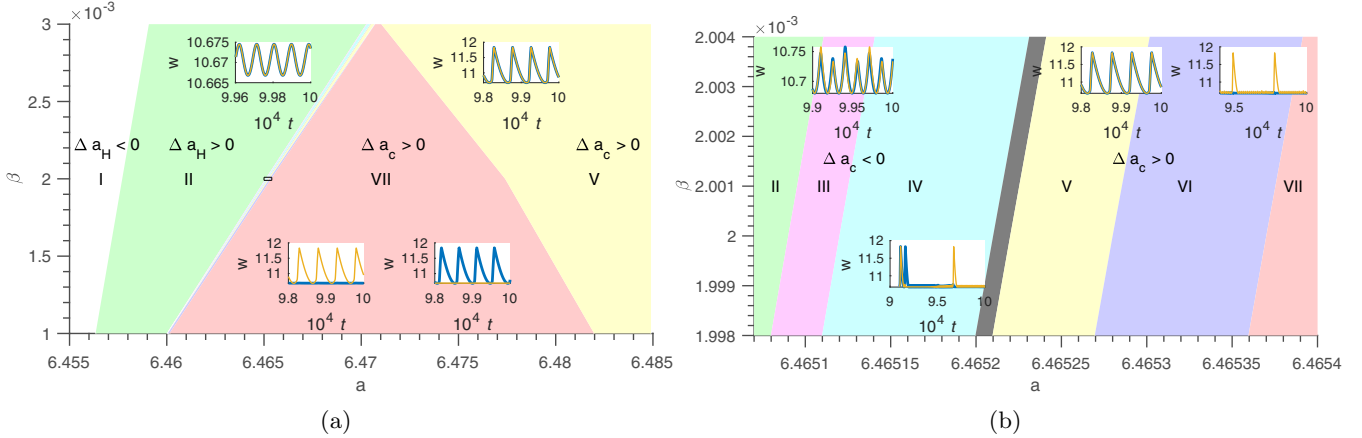


FIG. 2. Two-parameter bifurcation diagram showing observations made varying  $a$  and  $\beta$  with different initial conditions with insets of time series for the different modes of oscillations. (I) Steady state. (II) Small amplitude oscillations. (III) Leapfrogging. (IV) Intermittent spiking. (V) Large-amplitude oscillations. (VI) MMOs with symmetry-breaking. (VII) Symmetry-breaking with switching. (a) Full diagram. (b) Blown up from Fig. 2(a). The black region in Fig. 2(b) represents the canard explosion.

a Hopf bifurcation, followed by a canard explosion giving rise to large-amplitude relaxation oscillations (LAO) as  $a$  is increased at fixed  $\beta$ . Figure 3 compares trajectories in the neighborhood of the canard when the system is started either with identical (top row) or with different (bottom row) initial conditions. At  $a = 6.460008$ , the oscillators exhibit in-phase small amplitude oscillations [Fig. 3(a)] when the initial conditions (ICs) are the same. With different ICs, the additional freedom available to the system in the full four-dimensional

phase space results in the leapfrogging SAOs seen in Region III of Fig. 2(b) and in Fig. 3(d) for the same value of  $a$ . At the canard critical point,  $a_c = 6.460010$ , the two oscillators with identical ICs explode from SAOs to LAOs, remaining in-phase as they turn right instead of left just above the minimum of the  $w$ -nullcline [Fig. 3(b)]. With different ICs the oscillators display intermittent spiking [Region IV of Fig. 2(b) and Fig. 3(e)] at this value of  $a$ , turning to the left at the elbow on most circuits, but occasionally turning to the right to

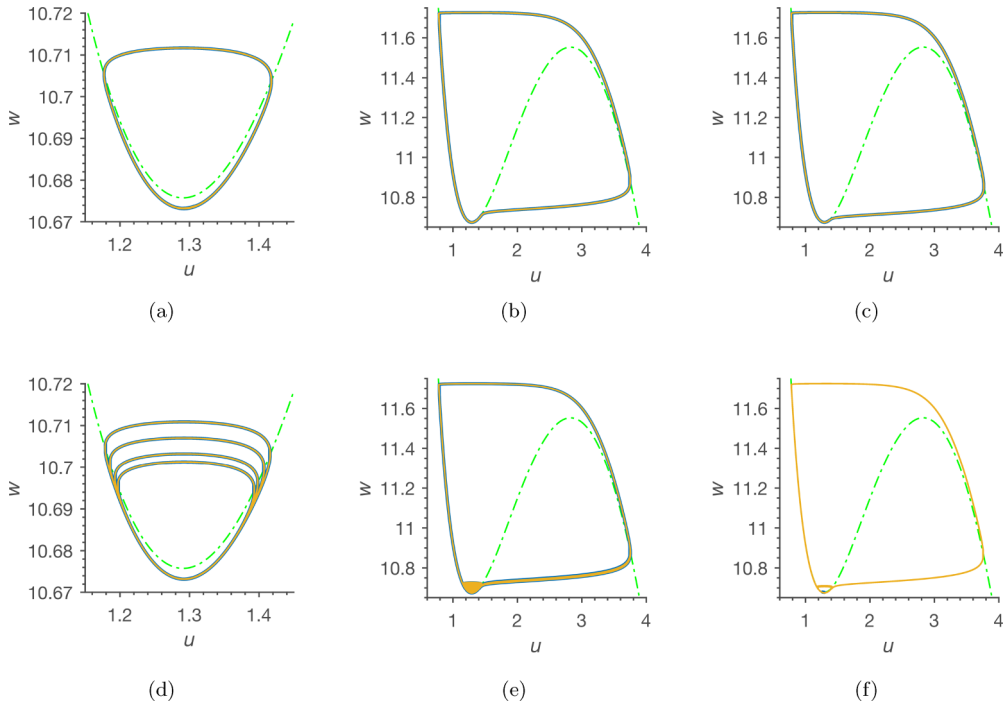


FIG. 3. Phase portraits of DC scheme showing numerical simulations with two different sets of initial conditions. Parameters:  $\beta = 0.001$  and  $D_v = 0.1552$ . Initial conditions: top panel  $(u_1, w_1) = (u_2, w_2) = (1.291, 10.68)$ , bottom panel  $(u_1, w_1) = (1.291, 10.68)$  and  $(u_2, w_2) = (3.00, 11.40)$ . (a) In-phase SAO at  $a = 6.460008$ . (b) In-phase LAO at canard critical point  $a = 6.460010$ . (c) In-phase LAO after canard at  $a = 6.460140$ . (d) Leapfrogging SAO at  $a = 6.460008$ . (e) Intermittent spiking at  $a = 6.460010$ . (f) MMOs after canard at  $a = 6.460140$ . Green (dashed):  $u$ -nullcline, yellow (dark gray): oscillator 1, yellow (light gray): oscillator 2. Where yellow and blue trajectories overlap, only gray is seen.

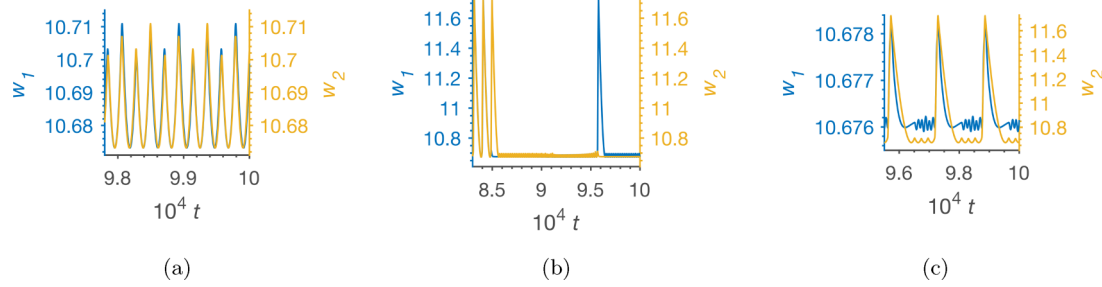


FIG. 4. Time series of DC scheme with  $D_v = 0.1552$  and  $\beta = 0.001$  obtained from numerical simulation. Initial conditions:  $(u_1, w_1) = (1.291, 10.68)$  and  $(u_2, w_2) = (3.0, 11.40)$ . (a) Leapfrogging SAO at  $a = 6.460008$  (4 peaks/period). (b) Intermittent spiking at  $a = 6.460030$ . (c) MMOs with symmetry-breaking at  $a = 6.460140$ . Oscillator 1 displays complex  $1^6$  MMOs while oscillator 2 displays simple  $1^3$  MMOs. Note change of scale. Blue (dark gray): oscillator 1, yellow (light gray): oscillator 2. Where yellow and blue trajectories overlap, only yellow is seen.

generate a spike. We observed in-phase oscillations [Fig. 3(c)] and mixed-mode oscillations [Region VI of Fig. 2(b) and in Fig. 3(f)] at  $a = 6.460140$ , for the same and different ICs, respectively.

Even if the initial conditions differ only very slightly, the behavior of the system becomes much richer than with identical ICs. The homogeneous in-phase LAO state exists for any value of  $\beta$  and is stable for most parameter sets. However, for each  $\beta$ , there is a narrow range of  $a$ , which shifts to higher  $a$  and broadens as  $\beta$  increases, in which this state becomes unstable. For example, at  $\beta = 0.001$ , the LAO is unstable for  $6.460003 \leq a \leq 6.460040$ , while at  $\beta = 0.002$ , the range of LAO instability is  $6.46509 \leq a \leq 6.46518$ . As  $a$  is increased starting from low values, the coupled system acts much like a single oscillator, first exhibiting a stable fixed point with equal concentrations for the two oscillators and then going through the Hopf bifurcation in a synchronized fashion. At or very near  $a_c$  for the uncoupled system, striking new behaviors emerge for the coupled system as noted above. These phenomena include leapfrogging (Fig. 4(a) and video 1 in the Supplemental Material [36]), in which both oscillators exhibit SAO, with one and then the other leading in phase as the amplitudes of successive spikes vary, allowing the oscillator with smaller amplitude to overtake the one with larger (but still small) amplitude; small amplitude chaos in both oscillators; and intermittent spiking [Fig. 4(b)], in which both oscillators primarily show SAO in an unsynchronized fashion, with one occasionally producing a large-amplitude spike. Leapfrogging typically sets in for  $a$  slightly below the  $a_c$  value for the uncoupled system, whereas intermittent spiking begins at the uncoupled value of  $a_c$  and continues until the canard critical value of the coupled system is reached. It is important to note that until the canard occurs the oscillators behave symmetrically, in the sense that both exhibit the same behavior, e.g., leapfrogging or intermittent spiking, even though they start from quite different initial conditions.

As  $a$  continues to increase, the system undergoes a canard explosion, with both oscillators transitioning to synchronized LAO. At slightly higher  $a$ , we observe PCSB, in which one oscillator maintains LAO, which may be singly or multiply periodic (mixed-mode), while the other exhibits SAO, typically mixed-mode. An example is shown in Fig. 4(c), where the LAO are simple  $1^3$ , in which the small oscillations are

roughly equal in amplitude, while the  $1^6$  mixed-mode SAO display a more complex structure.

A notable phenomenon, which occurs at  $\beta = 0.003$ , is a sudden switch between the two oscillators on increasing  $a$ . For example, at  $a = 6.47074$  ( $\Delta a_c > 0$ ) oscillator 2 exhibits large-amplitude singly periodic oscillations, whereas oscillator 1 oscillates with small amplitude and period-4 [see time series in Fig. 5(a) and next-amplitude (1D) map in Fig. 5(b)]. When  $a$  is increased to 6.47075, the oscillators reverse roles. On further increasing  $a$ , the oscillators reverse roles again. This switching behavior is significant, because it constitutes an exception to our earlier observation that, for most parameter values, symmetry-breaking results in the oscillator that starts in the vicinity of the large limit cycle becoming the large-amplitude oscillator. Here, that memory of initial conditions appears to be lost, or more accurately, reversed, implying a complex interaction between initial conditions, parameter values and the diverging trajectories that result in the canard phenomenon.

At higher  $a$ , the oscillators resynchronize and display in-phase LAO, whose amplitude increases with  $a$ . The results are summarized in Table I in the Supplemental Material [36] for several values of  $\beta$ .

We next examine the effect of varying the coupling strength,  $D_v$ , near the canard critical value ( $a_c$ ) of the uncoupled system. At very low values of  $D_v$ , we expect the two oscillators to behave as individual oscillators. On the other hand, for very high values of  $D_v$ , the two oscillators act as a single oscillator. Figures 6(a)–6(h) show various MMOs obtained as  $D_v$  increases for three values of  $a$ . We find “three-way MMO” patterns shown in Fig. 6(a) and Figs. 6(d) and 6(e), in which each oscillator exhibits maxima with small, medium, and large amplitude in each cycle. Figure 6(a) shows each oscillator going through a large, two small and one medium excursion in each cycle. The phase portrait in video 2 (in the Supplemental Material [36]) shows an apparent reversal of direction in the three-way MMOs during the medium-amplitude excursion. The two oscillators are nearly in-phase during the small excursions. As they begin to make the large excursions, one oscillator is seen to reverse direction in the  $u$ - $w$  plane. Both oscillators increase in amplitude with respect to the  $w$  variable. The large-amplitude oscillator, however, increases in  $u$  while the medium-amplitude oscillator decreases in  $u$ . As  $D_v$  increases further, we observe  $1^3$  MMOs with symmetry-breaking as

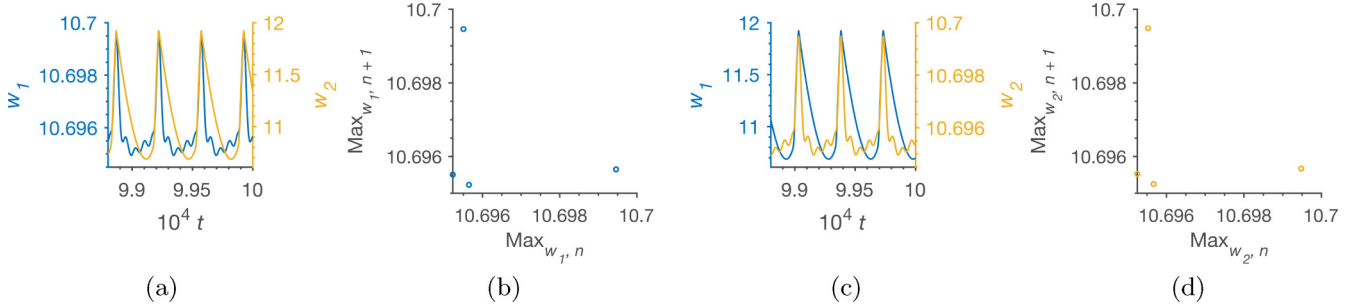


FIG. 5. Numerical simulations of DC scheme with  $D_v = 0.1552$  and  $\beta = 0.003$ . Initial conditions: (a)  $(u_1, w_1) = (1.291, 10.68)$  and  $(u_2, w_2) = (3.0, 11.40)$ . (a) LAO for oscillator 2 and SAO for oscillator 1 at  $a = 6.47074$ . (b) Next-amplitude map of oscillator 1 from Fig. 5(a). (c) LAO for oscillator 1 and SAO for oscillator 2 at  $a = 6.47075$ . (d) Next-amplitude map of oscillator 2 from Fig. 5(c). Blue (dark gray): oscillator 1, yellow (light gray): oscillator 2. Where yellow and blue trajectories overlap, only yellow is seen.

shown in Fig. 6(b). Both oscillators display  $1^3$  MMs, with one of the oscillators having half the amplitude of the other. As  $D_v$  increases, there is a switch as shown in Fig. 6(c), where the oscillators reverse roles while maintaining the  $1^3$  MMs with

symmetry-breaking. With  $a = 6.460080$  and  $\beta = 0.001$ , we obtain the behavior shown in the bottom panel of Fig. 6, which resembles that seen in Fig. 4(c), where oscillator 2 displays

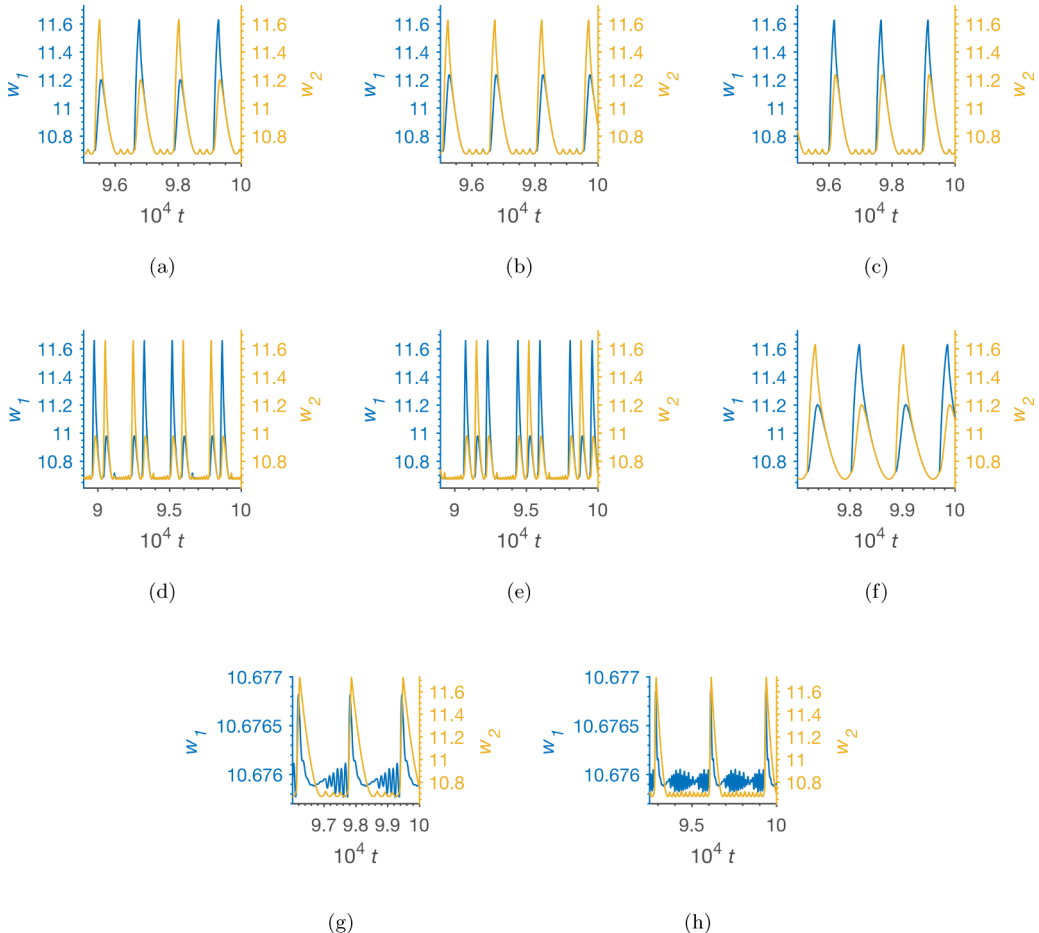


FIG. 6. Numerical simulations of DC time series with  $\beta = 0.001$ . Initial conditions: (a)  $(u_1, w_1) = (1.291, 10.68)$  and (b)  $(u_2, w_2) = (3.0, 11.40)$ . Top panel:  $a = 6.46000$ , middle panel:  $a = 6.46001$ , bottom panel:  $a = 6.46008$ . (a) Three-way MMs at  $D_v = 10$ . (b) MMs with symmetry-breaking (oscillator 2 red) at  $D_v = 11.0855$ . (c) MMs with symmetry-breaking (oscillator 1 blue) at  $D_v = 11.0990$ . (d) Three-way MMs at  $D_v = 4.981$ . (e) Three-way MMs with  $D_v = 4.985$ . (f) Nearly in-phase oscillations at  $D_v = 10$ . (g)  $1^3$  simple MMs for oscillator 2 and  $1^{10}$  complex MMs for oscillator 1 at  $D_v = 0.0824$ . (h)  $1^{10}$  simple MMs for oscillator 2 and  $1^{24}$  complex MMs for oscillator 1 at  $D_v = 0.0848$ . Blue (dark gray): oscillator 1, yellow (light gray): oscillator 2. Where yellow and blue trajectories overlap, only yellow is seen.

TABLE II. Notable observations for the diffusively coupled system with  $\beta = 0.002$  and  $a = 6.46513$ 

Case	$D_v$	Oscillator 1	Oscillator 2
1	0–0.00007	LAO	LAO
2	0.00008–0.014	LAO, intermittent spiking	LAO, intermittent spiking
3	0.015	LAO	SAO
4	0.9105–1.182	QP <sup>a</sup> SAO (smaller)	QP SAO
5	1.598	Simple MMOs (large)	Complex MMOs (small)
6	1.599–1.601	Complex MMOs (small)	Simple MMOs (large)
7	1.604	Antiphase MMOs	Antiphase MMOs

<sup>a</sup>Quasiperiodic.

simple 1<sup>3</sup> MMOs while oscillator 1 exhibits more complex MMOs.

Table II summarizes results for  $\beta = 0.002$  and  $a = 6.46513$ , which is the canard critical point for the uncoupled system. We find intermittent spiking with one of the oscillators [Fig. 7(a)], while the other exhibits LAOs. Symmetry-breaking occurs with an increase in  $D_v$  as shown in Fig. 7(b) with oscillator 1 showing LAOs as oscillator 2 undergoes period-5 SAOs. This phenomenon occurs only in a small range of  $D_v$ . At  $D_v = 0.9105$ , the two oscillators transition to small-amplitude, symmetry-broken, quasiperiodic oscillations similar to Fig. 12(b). This state continues up to  $D_v = 1.182$ . The oscillators resynchronize and oscillate with large amplitude at higher values of  $D_v$ .

## B. Modified subsystems

To obtain further insight into the observed behavior, we carry out a series of calculations in which we simplify the full diffusively coupled (DC) model by considering only a subset of the coupling terms. We describe these modified models below.

### 1. Self-disinhibition

Rotstein *et al.* [20,37] obtained insight into the origin of localized clusters in systems of globally coupled oscillators by

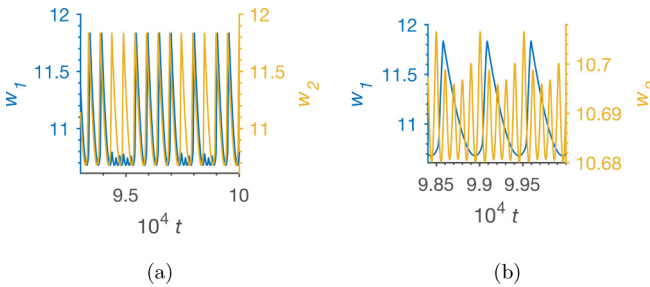


FIG. 7. Time series for DC system with constant  $a$  and  $\beta$  obtained from numerical simulation for varying  $D_v$ . Parameters:  $a = 6.46513$  and  $\beta = 0.002$ . Initial conditions:  $(u_1, w_1) = (1.291, 10.68)$  and  $(u_2, w_2) = (3.0, 11.40)$ . (a) LAO for oscillator 2 and intermittent spiking for oscillator 1 at  $D_v = 0.00007$ . (b) Symmetry-breaking, oscillator 1 (LAO), oscillator 2 (SAO, 5 peaks per period) at  $D_v = 0.015$ . Blue (dark gray): oscillator 1, yellow (light gray): oscillator 2. Where yellow and blue trajectories overlap, only blue is seen.

separating the coupling into autonomous and nonautonomous terms. They then viewed the uncoupled, autonomous system, which includes only the self-disinhibition portion of the full coupling as being forced by the nonautonomous terms. We adopt a similar approach here and first focus on the autonomous part of Eq. (23), given by Eq. (25). The remaining nonautonomous terms in Eq. (23) represent the forcing or cross-coupling exerted on oscillator  $i$  by the other oscillator. We analyze Eq. (25) in Appendix B to obtain expressions for the Hopf [Eq. (B6)] and canard critical points [Eq. (B7)] as well as the steady state (Appendix C), all of which shift as a result of the self-disinhibition. The minimum in the nullcline,  $u_m$ , is unchanged from its uncoupled value.

$$\begin{aligned} \frac{du_i}{dt} &= a - u_i - \frac{u_i(u_i\beta + w_i)}{1 + u_i^2}, \\ \frac{dw_i}{dt} &= \beta[5u_i - a - D_v(\beta u_i + w_i)], \\ i &= 1, 2. \end{aligned} \quad (25)$$

Table III compares the canard critical points from simulations to those predicted from KS analysis of Eq. (25) for different values of  $\beta$ .

### 2. Cross-coupling

In the cross-coupling (CC) scheme, each oscillator provides a forcing (the nonautonomous part) to the other, but we neglect the self-disinhibition terms. The system evolves as shown in Eq. (26),

$$\begin{aligned} \frac{du_i}{dt} &= a - u_i - \frac{4u_i v_i}{1 + u_i^2}, \\ \frac{dv_i}{dt} &= \beta \left[ u_i - \frac{u_i v_i}{1 + u_i^2} + D_v v_j \right], \end{aligned} \quad (26)$$

where  $i \neq j$ .

TABLE III. Predicted Hopf bifurcation and canard critical point of the diffusively coupled LE system with  $D_v = 0.1552$

$\beta$	$a_H$ LSA	$u_{m_H}$	$a_c$ sim	$u_{m_c}$	$\lambda_c$ pre	$\lambda_c$ sim
0.001	6.45581	1.29116	6.46005	1.29074	$1.28 \times 10^{-3}$	$1.27 \times 10^{-3}$
0.002	6.45664	1.29133	6.46522	1.29047	$2.56 \times 10^{-3}$	$2.57 \times 10^{-3}$
0.003	6.45747	1.29150	6.47050	1.29020	$3.82 \times 10^{-3}$	$3.90 \times 10^{-3}$
0.004	6.45831	1.29166	6.47591	1.28991	$5.06 \times 10^{-3}$	$5.28 \times 10^{-3}$

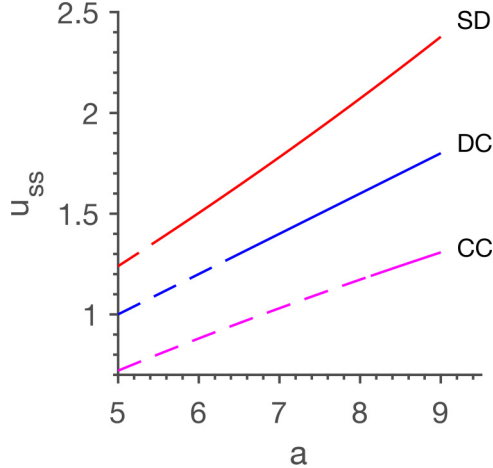


FIG. 8. Stability of steady states of DC, SD, and CC with  $D_v = 0.1552$  varying  $a$ . Dashed lines represent stable steady states, and solid lines correspond to unstable steady states.

In the new variables, we have

$$\begin{aligned} \frac{du_i}{dt} &= a - u_i - \frac{u_i(u_i\beta + w_i)}{1 + u_i^2}, \\ \frac{dw_i}{dt} &= \beta[5u_i - a + \beta D_v u_j + D_v w_j]. \end{aligned} \quad (27)$$

At the steady state,  $u_i = u_j$  and  $w_i = w_j$ . As shown in Appendix C, the SD and CC schemes shift the position of the steady state from the DC values in opposite directions by

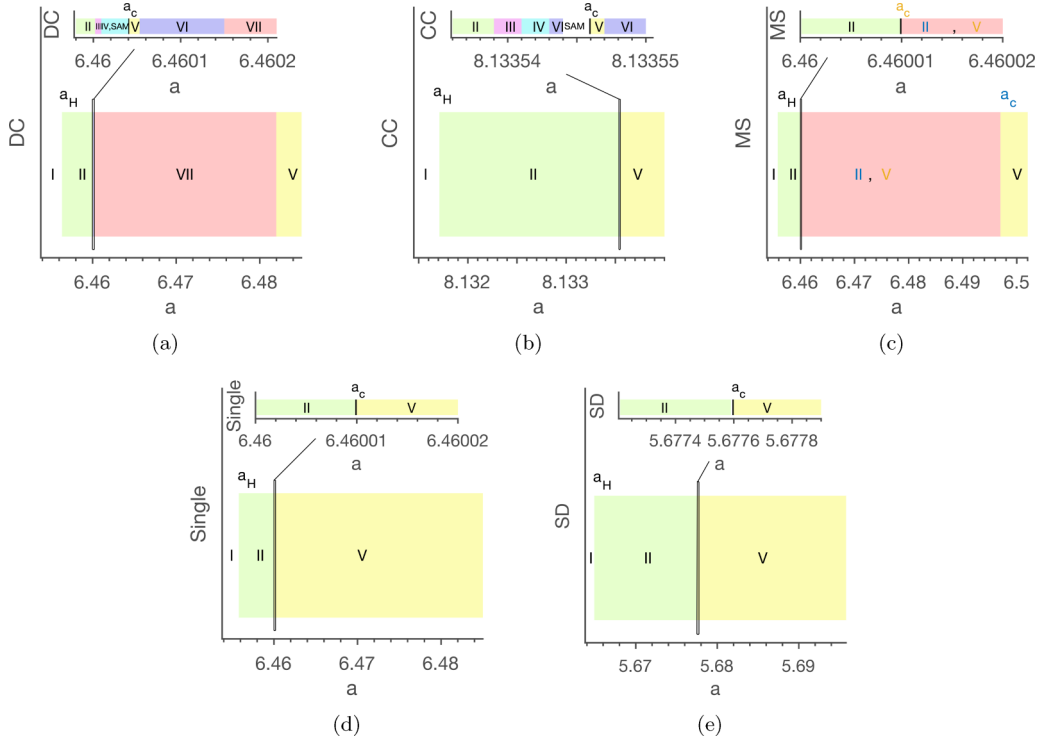


FIG. 9. Bifurcation diagrams of DC, CC and MS schemes with  $D_v = 0.1552$  and  $\beta = 0.001$  obtained from numerical simulation. Initial conditions:  $(u_1, w_1) = (1.291, 10.68)$  and  $(u_2, w_2) = (3.0, 11.40)$ . (a) DC, (b) CC, (c) MS, (d) Single, (e) SD. Regions are numbered as in Fig. 2.

nearly equal amounts. Figure 8 compares the steady states and their stability for the DC, SD and CC coupling schemes.

### 3. Master-slave (one-way coupling)

In the master-slave (MS) scheme, we set  $D_v = 0$  for  $dw_2/dt$  in Eq. (23), so that one of the oscillators (2, the master) influences the other (1, the slave) but receives no input from the slave. We seek to understand the origin of the symmetry-breaking as well as other patterns observed. Can the master suppress the slave? And if so, could this be the reason for the patterns we find? We compare the results for the various coupling schemes in Sec. IV.

## IV. COMPARISON OF SUBSYSTEMS

In an effort to determine the origin of the patterns and PCSB seen with the full DC scheme, we compare the different coupling schemes by varying  $a$  and then  $D_v$ .

### A. Varying $a$

We first fix  $D_v = 0.1552$  and  $\beta = 0.001$  and vary  $a$ . Figure 9 and Table II (in the Supplemental Material [36]) compare the four coupling schemes to the uncoupled system. Figure 10 shows selected time series of the DC, CC, and MS systems. All schemes have the oscillators at steady states at low values of  $a$  (Region I). As  $a$  increases, harmonic SAOs appear through a supercritical Hopf bifurcation (Region II of Fig. 9 and Table II in the Supplemental Material [36]). The DC and CC schemes show similar patterns with increasing  $a$ . For instance, both schemes display leapfrogging at

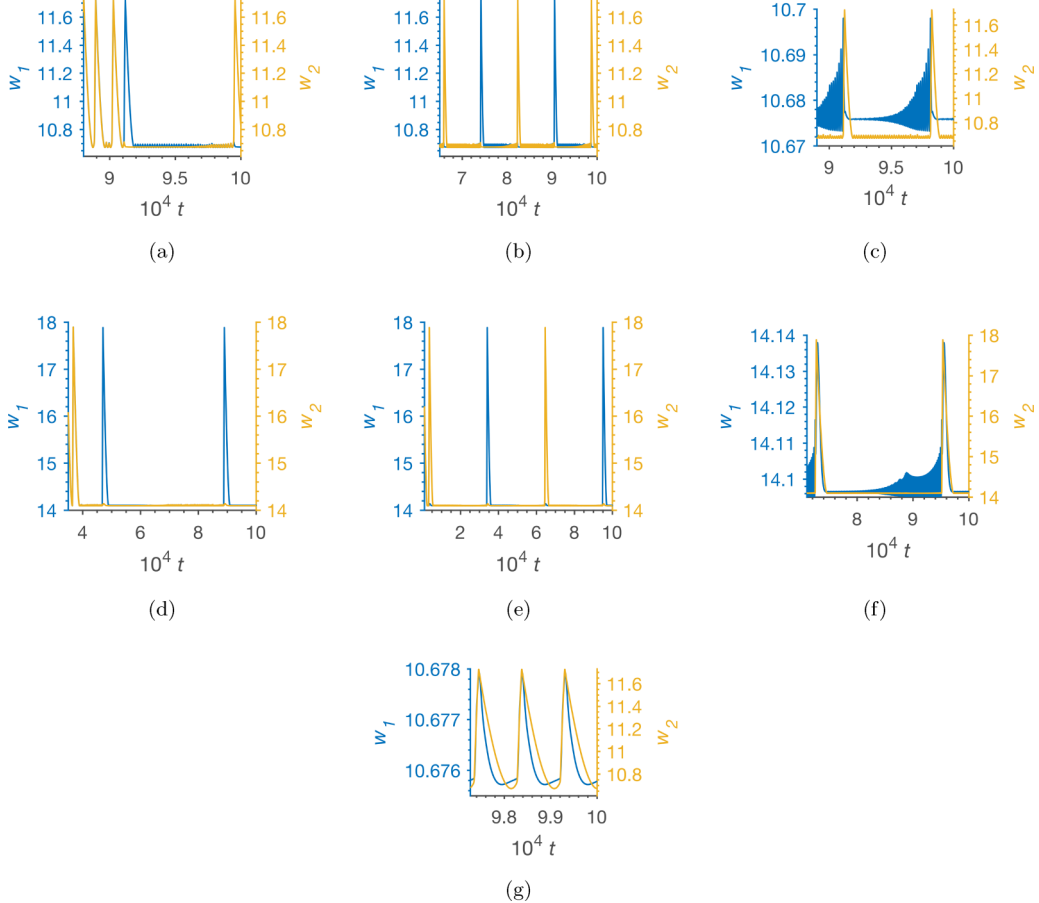


FIG. 10. Examples of time series of DC (top panel), CC (middle panel), and MS (bottom panel) schemes with  $D_v = 0.1552$  and  $\beta = 0.001$  obtained from numerical simulation with regions similar to those in Fig. 2. Initial conditions:  $(u_1, w_1) = (1.291, 10.68)$  and  $(u_2, w_2) = (3.0, 11.40)$ . (a) Intermittent spiking at  $a = 6.460013$ . (b) Simple antiphase MMOs at  $a = 6.460016$ . (c) MMOs with symmetry-breaking at  $a = 6.460053$  with simple MMOs for oscillator 2 and complex MMOs for oscillator 1. (d) Intermittent spiking at  $a = 8.133542$ . (e) Simple antiphase MMOs at  $a = 8.133545$ . (f) MMOs with symmetry-breaking at  $a = 8.133547$  with simple MMOs for oscillator 2 and complex MMOs for oscillator 1. (g) Period-1 with symmetry-breaking at  $a = 6.460010$ . Blue (dark gray): oscillator 1, yellow (light gray): oscillator 2. Where yellow and blue trajectories overlap, only yellow is seen.

$\Delta a_c < 0$  (Region III of insets) as well as intermittent spiking (Region IV of insets) as shown in Figs. 10(a) and 10(d) for DC and CC, respectively. Another similarity between the two coupling schemes is the presence of simple antiphase MMOs where both oscillators display similar patterns with both small excursions and large-amplitude oscillations as shown in Figs. 10(b) and 10(e) [denoted SAM in the insets of Figs. 9(a) and 9(b)]. In both schemes they occur at  $\Delta a_c < 0$ . We observe PCSB [Fig. 10(c)] for DC and [Fig. 10(f)] for CC. After the canard explosion, with increasing  $a$ , the two oscillators display symmetry-breaking with simple MMOs for one oscillator (mixture of large and small amplitude for oscillator 2) and complex MMOs for the other (only small amplitude for oscillator 1), similar to Fig. 4(c). We note that all the MMOs with symmetry-breaking for DC occur at  $\Delta a_c > 0$ , whereas for CC we find them both at  $\Delta a_c < 0$  and  $\Delta a_c > 0$ , as shown as Region VI of the insets in Figs. 9(a) and 9(b), respectively. The SD scheme shows a steady state, Hopf bifurcation, SAO, and canard explosions ( $a_c = 5.6775$ ) but fails to exhibit PCSB. The MS model does not show leapfrogging but displays various quasiperiodic oscillations as well as small-amplitude chaos in the slave oscillator. We

did not observe this behavior with either the SD or the CC scheme, but did find it in the DC system, just before the intermittent spiking. Another pattern found in both the DC and MS models is symmetry-breaking with period-1 LAO for oscillator 2 and period-1 SAO for oscillator 1. As  $a$  increases, we occasionally see the oscillators transitioning to large-amplitude in-phase periodic oscillations before returning to symmetry-breaking. This kind of intermittent transition from MMOs with symmetry-breaking to in-phase LAOs occurs in the range  $6.460053 < a < 6.46014$  for DC. It implies that our initial condition for oscillator 1 lies near the boundary of the basin of attraction of the MMOs, which shifts as  $a$  is varied.

The lack of simple MMOs, antiphase MMOs and MMOs with symmetry-breaking in the SD and MS coupling schemes and their presence in the CC scheme suggests that they arise in DC as the result of the cross-coupling term. Also, the presence of period-1 symmetry-breaking and the absence of the other observable patterns in the master-slave model supports the notion that the post-canard symmetry-breaking arises from one of the oscillators (oscillator 2) forcing or slaving the other (oscillator 1). This implies that, even in the CC scheme, one oscillator continuously forces the other.

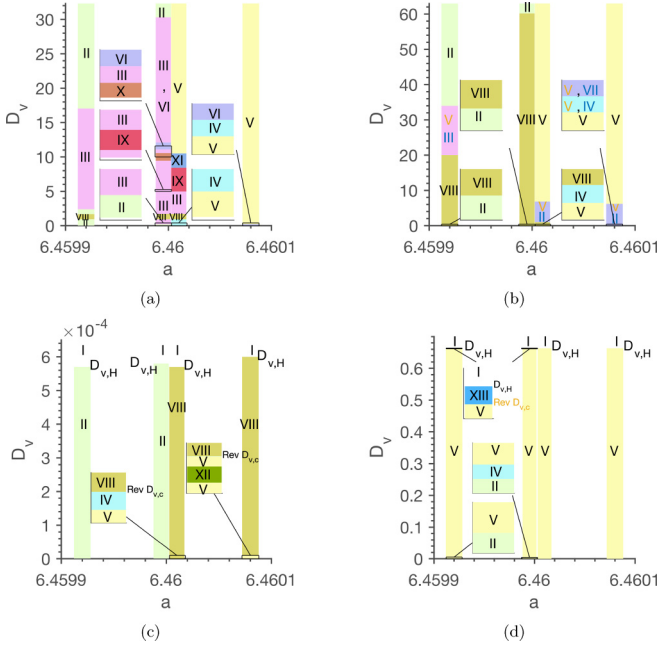


FIG. 11. Two-parameter bifurcation diagram varying  $D_v$  at four values of  $a$  with  $\beta = 0.001$  constructed from Tables III-VI (in the Supplemental Material [36]) for the different coupling schemes. The regions are: steady state (I), SAO (II), leapfrogging (III), intermittent spiking (IV), LAO (V), MMO with symmetry-breaking (VI), symmetry-breaking with switching (VII), SAO with symmetry-breaking (VIII), antiphase triperiodic (IX), three-way MMOs (X), antiphase (XI), simple MMOs (XII), and symmetry-breaking with LAOs for oscillator 1 and steady state for oscillator 2 (XIII). (a) DC, (b) MS, (c) CC, (d) SD.

At high values of  $a$ , all four coupling schemes settle into LAOs, which are in-phase for DC, CC, and MS. With SD, the oscillators are decoupled, so at large  $a$  they oscillate with the same amplitude and period with a phase difference determined by the initial conditions.

### B. Varying $D_v$

We next compare the coupling schemes using constant  $a$  and  $\beta$ , varying  $D_v$ . We set  $\beta = 0.001$  and choose  $a$  for the uncoupled system before the canard explosion,  $\Delta a_c < 0$  ( $a = 6.45992, 6.46000$ ), at the canard explosion,  $\Delta a_c = 0$  ( $a = 6.46001$ ) and after the canard explosion  $\Delta a_c > 0$  ( $a = 6.46008$ ). We seek to illuminate the effect of increasing the coupling strength on the system.

At  $D_v = 0$ , all schemes show SAO for both oscillators with a phase difference determined by the initial conditions for  $a = 6.45992$  [Region II Figs. 11(a)–11(d)]. As  $D_v$  increases, DC, MS, and CC display more complex SAO. For example, the DC system exhibits symmetry-breaking with SAO consisting of combinations of periodic, quasiperiodic and chaotic oscillations at various values of  $D_v$  [Region VIII of Fig. 11(a)]. At other  $D_v$ , it shows leapfrogging as well as in-phase SAO where the oscillators oscillate with the same amplitude, period and phase (Regions III and II, respectively). The CC scheme, on the other hand, displays only simple SAO and goes to a steady state through a Hopf bifurcation as  $D_v$  increases. The slave in the MS scheme exhibits patterns similar to those obtained

with the DC system. For example, we observe SAO with periodic, quasiperiodic, and chaotic oscillations at various values of  $D_v$  (Region VIII). The SD scheme, unlike the others, shows a significant range of LAO after a brief period of SAO. A canard explosion occurs at  $D_v = 0.0000127$  [Fig. 12(b)] with  $\lambda_c = 0.00126$ . This scheme also exhibits PCSB where oscillator 2 undergoes SAO while oscillator 1 continues with LAO [see Region XIII of Fig. 11(d)]. To better gain insight into the origin of the LAO and PCSB for this scheme with this choice of  $a$ , we look at the phase portraits where these patterns arise (Fig. 12). The  $u$ -nullcline is independent of the coupling strength. The  $w$ -nullcline, however, is affected by changing  $D_v$ . As  $D_v$  increases, the  $w$ -nullcline shifts from left to right, changing the position of the fixed point. The phase portrait appears almost symmetric at  $D_v = 0.3$  [Fig. 12(c)]. Just before the symmetry-breaking, the fixed point is found near the maximum of the  $u$ -nullcline [Fig. 12(d)]. As  $D_v$  increases, oscillator 1 maintains its large-amplitude relaxation oscillations while oscillator 2 goes to a steady state, resulting in PCSB. Thus the origin of the PCSB in this case appears fundamentally different from that observed in the other coupling schemes, since here it is related to the shift of the fixed point from the minimum to the maximum in the  $u$ -nullcline. There is bistability between the steady state and a stable limit cycle oscillation.

In the CC scheme, on the other hand, the  $w$ -nullcline moves from right to left with increasing  $D_v$ , eventually falling to the left of the minimum of the cubic nullcline, thereby passing through the Hopf bifurcation [Figs. 12(f) and 12(g)].

The DC and MS coupling schemes resemble one another with regard to the patterns observed and the lack of steady-state behavior at higher coupling strengths. In both schemes, the (homogeneous) fixed point is independent of the coupling strength. In Fig. 13, the top and bottom panels show some of the patterns found for the DC and MS schemes, respectively. The oscillators display small-amplitude quasiperiodic oscillations with oscillator 1 having a smaller amplitude than oscillator 2, as shown in Fig. 13(a) for DC and Fig. 13(d) for MS. As  $D_v$  increases, the oscillators oscillate with a single period in both schemes, as shown in Figs. 13(b) and 13(e), for DC and MS, respectively. The DC scheme displays leapfrogging at  $D_v = 3.50$ , as shown in Fig. 13(c). We observe something similar to leapfrogging in the MS scheme when the slave oscillator exhibits period-2 oscillations [see Fig. 13(f)], while the master oscillations are simply periodic with an amplitude intermediate between those of the alternating peaks of the slave oscillator. For  $D_v > 17.04$ , the DC system settles into in-phase SAO, which occurs for  $D_v > 33.904$  for the MS scheme. We do not observe any LAO, intermittent spiking or symmetry-breaking with either simple or complex MMOs for any of the  $D_v$  values studied for the DC, MS and CC schemes at this value of  $a$ .

Next, we study the behavior of the oscillators just before the canard explosion at  $a = 6.46000$ . The results obtained are shown in Table IV (in the Supplemental Material [36]). At  $D_v = 0$ , the oscillators are in the small-amplitude oscillatory regime for all coupling schemes. As  $D_v$  increases, various oscillatory patterns emerge. Unlike the behavior at  $a = 6.45992$  where the DC, CC and MS schemes exhibit only variations of SAO, at  $a = 6.46000$  as  $D_v$  increases, we also find patterns

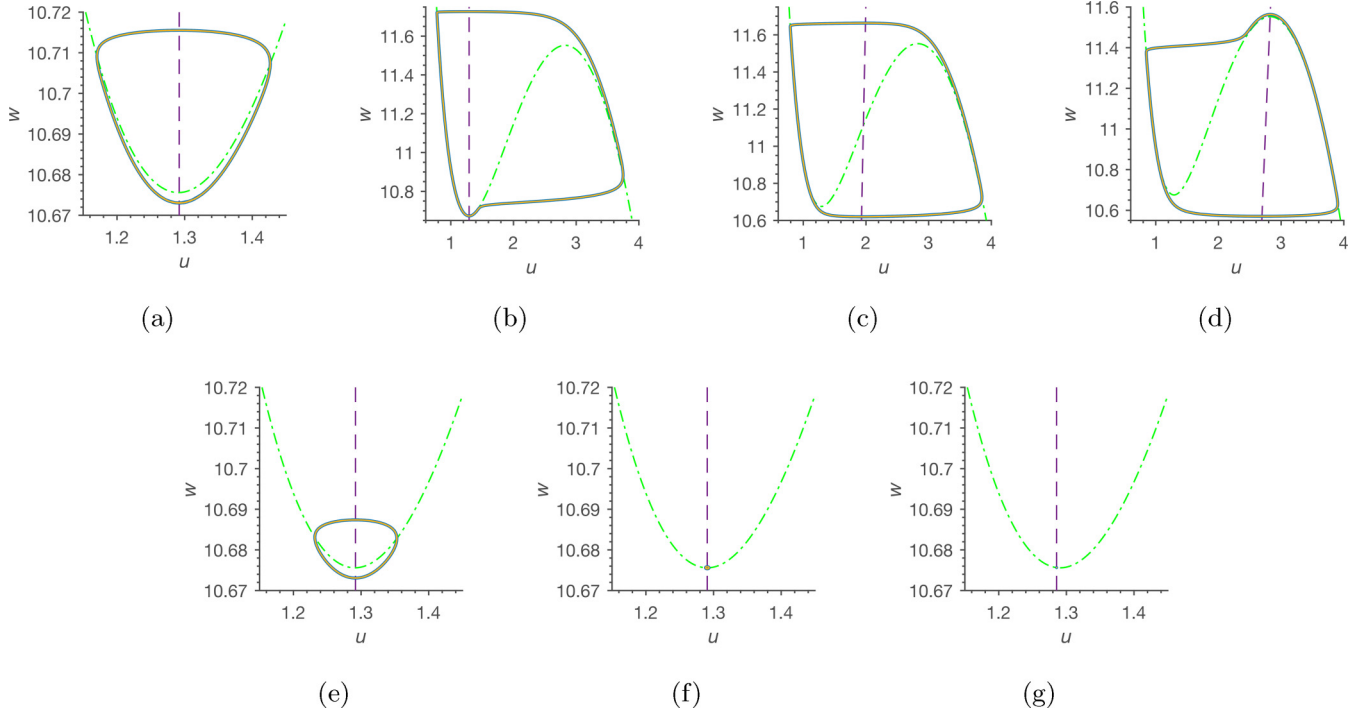


FIG. 12. Numerical simulations of phase portraits of SD and CC schemes with  $a = 6.45992$  and  $\beta = 0.001$ . Initial conditions:  $(u_1, w_1) = (1.291, 10.68)$  and  $(u_2, w_2) = (3.0, 11.40)$ . Top row: SD, bottom row: CC. (a) In-phase SAO at  $D_v = 0.0000126$  (note the scale). (b) In-phase LAO at  $D_v = 0.0000127$  immediately after the canard explosion. (c) In-phase LAO at  $D_v = 0.3$ . (d) In-phase LAO at  $D_v = 0.663058$  before the symmetry-breaking. (e) In-phase SAO at  $D_v = 0.0001$ . (f) Hopf bifurcation  $D_v = 0.00058$ . (g) Fixed point at  $D_v = 0.003$ . Dashed-dotted green lines:  $u$ -nullcline, purple dashed lines:  $w$ -nullcline, blue (dark gray) line: oscillator 1; yellow (light gray): oscillator 2. Where yellow (light gray) and blue (dark gray) trajectories overlap, only gray is seen.

that contain large-amplitude relaxation oscillations, presumably because the system now lies very close to the canard critical point of the uncoupled system.

The SD scheme shows intermittent spiking with  $D_v = 0.00000014$ . The CC and MS schemes behave much as they did

for  $a = 6.45992$ . At sufficiently high  $D_v$ , the oscillators settle into in-phase SAO, reflecting the fact that a single oscillator shows SAO at this value of  $a$ .

Just beyond the canard point, at  $a = 6.46001$ , all coupling schemes display LAO for  $D_v = 0$ . Figures 6(d)–6(f) show

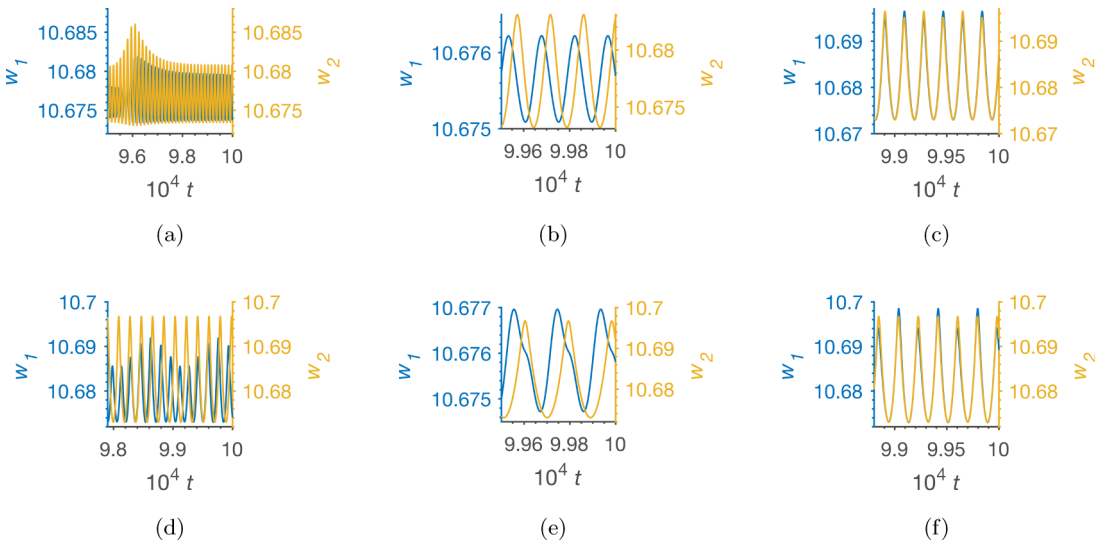


FIG. 13. Time series of DC and MS schemes with  $a = 6.45992$  and  $\beta = 0.001$  obtained from numerical simulation. Initial conditions:  $(u_1, w_1) = (1.291, 10.68)$  and  $(u_2, w_2) = (3.0, 11.40)$ . Top panel: DC, bottom panel: MS. (a) Quasiperiodic oscillations at  $D_v = 0.9298$ . (b) Singly periodic oscillations at  $D_v = 1.35$ . (c) Leapfrog at  $D_v = 3.50$ . (d) Quasiperiodic oscillations at  $D_v = 0.131$ . (e) Singly periodic oscillations at  $D_v = 3.50$ . (f)  $1^1$  oscillations for osc. 1, period-1 for osc. 2 at  $D_v = 25.00$ . Blue (dark gray): oscillator 1; yellow (light gray): oscillator 2. Where yellow and blue trajectories overlap, only yellow is seen.

several interesting patterns as seen for DC as  $D_v$  is increased. In contrast to the behavior at  $a = 6.46000$ , which lies just before the canard point for the single oscillator and exhibits patterns in which the oscillators predominantly show SAO, the DC system is now dominated by patterns in which the oscillators spend most of their time in LAO, composed of different variations of mixed-mode leapfrog oscillations with occasional small-amplitude oscillations. The CC scheme also shows intermittent spiking after a brief interval of LAO (Table V). We observe small-amplitude chaos, which is also found for DC.

As  $D_v$  increases, the CC oscillators undergo a reverse canard explosion, accompanied by intermittent spiking and PCSB, to SAO, followed by a Hopf bifurcation to the steady state. Again the sequence of LAO, intermittent spiking, small-amplitude chaotic oscillation, and steady state in-phase SAO results from the shift of the  $w$ -nullcline from right to left as  $D_v$  increases. The MS scheme behaves much like the DC scheme for this value of  $a$ , displaying intermittent spiking for the slave oscillator as well as complex symmetry-breaking and a return to LAO at very strong coupling. In general, the strong coupling and weak coupling limits in DC and MS behave nearly identically, since the system behaves like a single oscillator in both limits. We note that the transitions in the MS scheme occur at significantly lower  $D_v$  than in the DC scheme, presumably because the two-way coupling in the latter scheme mitigates the effect of the pure forcing in the MS.

The SD scheme displays LAO and symmetry-breaking, much as occurs with  $a = 6.45992$  and  $a = 6.46000$ . The absence of SAO for this scheme results from the rightward shift of the  $w$ -nullcline with increasing  $D_v$ .

At  $a = 6.46008$ , the oscillators are in the LAO regime for  $D_v = 0$ . For DC, we observe various MMOs with symmetry-breaking consisting of multiple small excursions before a large spike with both oscillators as shown in Table VI (in the Supplemental Material [36]). Fig. 6(g), for example, displays a pattern in which oscillator 2 shows  $1^3$  MMOs whereas oscillator 1 undergoes  $1^{10}$  small-amplitude MMOs. The number of small excursions between large excursions increases with increasing  $D_v$ , as shown in Table VI in the Supplemental Material [36] and Fig. 6(h). The CC scheme shows various MMOs ( $1^1$ ,  $1^2$ , etc.) as  $D_v$  increases [Region XII of Fig. 11(c)]. For the MS model we observe a sizable range of  $D_v$  (0.0028 - 6.1831) over which the small-amplitude oscillator 1 undergoes periodic oscillations with the number of peaks per period decreasing with  $D_v$ . This behavior appears to correspond to the complex MMOs observed in the DC scheme for  $0.0824 < D_v < 0.20338$ . The SD scheme behaves much as it did for  $a = 6.46001$ , i.e., LAO followed by steady state.

At all the  $a$  values considered, varying  $D_v$  fails to produce MMOs with either the SD or MS coupling schemes. Only DC and CC appear to be capable of generating mixed-mode behavior.

The canard critical and reverse canard points ( $\lambda_c$ ) obtained from numerical simulations while varying  $D_v$  at  $\beta = 0.001$  stay at  $\lambda_c = 0.00126$  for the DC, CC and MS coupling schemes. The canard explosion for SD with  $\beta = 0.001$  for  $a = 6.45992$  and  $a = 6.46$  occurs at  $D_v = 0.0000127$  and 0.0000015, respectively. Both have  $\lambda_c = 0.00126$ .

## V. DISCUSSION AND CONCLUSIONS

We analyzed the diffusively coupled system by breaking it into subsystems to identify the origin of the exotic patterns as well as the PCSB observed. Varying  $a$  and  $D_v$  for the self-disinhibition coupling scheme did not reveal any exotic patterns or PCSB. We only found SAO, LAO, intermittent spiking, Hopf bifurcation and steady state. The oscillators in this coupling scheme are uncoupled and thus act like a modified single oscillator system with the position of the steady state shifted.

With CC, we observed many patterns similar to those observed in DC. Most of the exotic patterns as well as the PCSB seen in DC were observed with CC when  $a$  was varied. For example, we found both antiphase MMOs and MMOs with symmetry-breaking for both coupling schemes. We also observed similarities between DC and CC when varying  $D_v$  for  $a$  above the canard critical value. For  $a$  below the canard explosion, varying  $D_v$  did not reveal any resemblance between DC and CC. We attribute this to the motion of the fixed point of the CC scheme with  $D_v$ . As  $D_v$  increases, the fixed point moves away (to the left) from the minimum of the  $u$ -nullcline, destabilizing the oscillatory behavior and resulting in a stable steady state. So, for  $a$  at or below the canard critical point only SAO and SS were seen.

For the MS model, we observed similarities with DC regarding the symmetry-breaking. At constant  $\beta$  and  $D_v$ , we saw symmetry-breaking where both oscillators oscillate with small amplitude (with the master having a slightly higher amplitude) when  $a$  is below the canard value of the uncoupled system. If  $a$  is chosen at or above  $a_c$  for the uncoupled system, then we observe a different form of symmetry-breaking in which there are large-amplitude oscillations for the master and small-amplitude oscillations for the slave. There are also similarities between DC and MS as we vary  $D_v$ , depending on whether  $a$  is pre-canard or post-canard for the uncoupled system. For example, for pre-canard values of  $a$ , we observe SAOs, symmetry-breaking, quasiperiodic oscillations and LAOs. For post-canard values of  $a$ , we observe in addition to intermittent spiking and LAO, symmetry-breaking with period-7, period-6, etc.

To conclude, we suggest that the exotic patterns observed in the DC system, notably the complex MMOs, arise from the cross-coupling and the influence that the oscillators exert on one another. Self-disinhibition appears to play a relatively minor role, primarily compensating for the shift in the steady state that would result in its absence from the pure cross-coupling term. We attribute the PCSB found in the DC primarily to the master-slave effect of the large-amplitude oscillator forcing the smaller one.

The results found here suggest several promising directions for further study. These include more detailed analysis of the origin of the phenomenon in the symmetry-broken patterns in which the small- and large-amplitude oscillators suddenly switch roles as a parameter is varied, and of the novel “three-way MMOs” observed in this study. Similar studies on other coupled oscillator models such as the FitzHugh-Nagumo or van der Pol models should shed light on the generality of the phenomena observed here. Finally, extending the system to more than two coupled oscillators is likely to reveal other novel dynamical behaviors.

## VI. NUMERICAL METHODS

Numerical simulations were carried out using MATLAB ODE solvers 45 and 113 for ODEs with absolute and relative tolerances of  $1 \times 10^{-9}$  and  $1 \times 10^{-12}$ , respectively. Results shown were obtained with MATLAB ODE solver 113. Simulations of results were done with a time span of  $1 \times 10^5$ . All analyses of results were done after eliminating initial transients.

## ACKNOWLEDGMENTS

This work was supported by the National Science Foundation under Grants No. CHE-1856484, No. DGE-1068620, and No. DMR-1420382. We thank H. Rotstein, M. Dolnik, and J. Touboul for useful comments and suggestions.

## APPENDIX A: KRUPA-SZMOLYAN CANARD ANALYSIS OF THE UNCOUPLED SYSTEM

To put the LE uncoupled system [Eq. (14)] into the canonical form, we shift and rescale  $(u, w, \lambda, t)$  to  $(x, y, \gamma, \tau)$  so that for singularity  $F(0, 0, 0) = F_x(0, 0, 0) = G(0, 0, 0) = 0$ . We also require  $F_{xx}(0, 0, 0) \neq 0$ ,  $F_y(0, 0, 0) \neq 0$ ,  $G_x(0, 0, 0) \neq 0$ , and  $G_\gamma(0, 0, 0) \neq 0$ . Let

$$\begin{aligned} x &= \alpha(u - u_m), & y &= \rho(w - w_m), \\ \gamma &= L\lambda, & \tau &= Tt, \end{aligned} \quad (\text{A1})$$

and

$$\begin{aligned} u &= \frac{x}{\alpha} + u_m, & w &= \frac{y}{\rho} + w_m, \\ \lambda &= \frac{\gamma}{L}, & t &= \frac{\tau}{T}. \end{aligned} \quad (\text{A2})$$

We need to find  $\alpha$ ,  $\rho$ ,  $L$ , and  $T$  so that Eq. (14) has the form of Eq. (15), i.e., in  $dx/d\tau$  in Eq. (15), there are no constants or terms proportional to  $x$ , and in Eq. (15) the constant terms in  $h_{1,2,4,5}$  are 1.

Substituting Eq. (A2) into Eq. (14),

$$\begin{aligned} \frac{T}{\alpha} \frac{dx}{d\tau} &= \left[ f_1 \left( \frac{x}{\alpha} + u_m, \beta \right) - \frac{y}{\rho} - w_m \right] f_2 \left( \frac{x}{\alpha} + u_m \right), \\ \frac{T}{\rho} \frac{dy}{d\tau} &= \beta \left[ 5 \left( \frac{x}{\alpha} + u_m - \frac{\gamma}{L} - u_m \right) \right] = \beta \left( \frac{5x}{\alpha} - \frac{5\gamma}{L} \right), \end{aligned} \quad (\text{A3})$$

or

$$\begin{aligned} \frac{dx}{d\tau} &= \frac{\alpha}{T} \left[ f_1 \left( \frac{x}{\alpha} + u_m, \beta \right) - \frac{y}{\rho} - w_m \right] f_2 \left( \frac{x}{\alpha} + u_m \right) \\ &\equiv \frac{\alpha}{T} f_3(x, y, \beta) f_2 \left( \frac{x}{\alpha} + u_m \right), \\ \frac{dy}{d\tau} &= \frac{\rho}{T} \beta \left[ 5 \left( \frac{x}{\alpha} + u_m - \frac{\gamma}{L} - u_m \right) \right] \\ &= \beta \left( \frac{5\rho}{T\alpha} x - \frac{5\rho}{TL} \gamma \right). \end{aligned} \quad (\text{A4})$$

Comparing Eq. (A4) with Eq. (15) gives

$$\begin{aligned} \frac{5\rho}{\alpha T} &= \frac{5\rho}{LT} = 1, \\ 5\rho &= \alpha T = LT, \end{aligned} \quad (\text{A5})$$

and

$$\begin{aligned} h_4 &= h_5 = 1, \\ h_6 &= 0 \text{ because } \frac{dy}{d\tau} \text{ is independent of } y. \end{aligned} \quad (\text{A6})$$

Note that the definition of  $(u_m, w_m)$  and the shift defined in Eq. (A1) guarantee that at  $x = y = 0$ , we have  $f_1(u_m, \beta) = w_m$ ,  $f_{1x}(u_m, \beta) = 0$ , so that  $f_3(0, 0, \beta) = f_{3x}(0, 0, \beta) = 0$ . We now need to put Eq. (A4) into canonical form. Expanding  $F$  around  $(0, 0, 0)$ , we write  $\bar{f} = f(0, 0)$  with a similar notation for derivatives evaluated at the origin:

$$\begin{aligned} \frac{dx}{d\tau} &= \frac{\alpha}{T} \left[ \bar{f}_2 \bar{f}_3 + (\bar{f}_{2x} \bar{f}_3 + \bar{f}_2 \bar{f}_{3x})x + \frac{1}{2}(\bar{f}_{2xx} \bar{f}_3 \right. \\ &\quad \left. + 2\bar{f}_{2x} \bar{f}_{3x} + \bar{f}_2 \bar{f}_{3xx})x^2 + \bar{f}_2 \bar{f}_{3y}y + \bar{f}_2 \bar{f}_{3\beta}\beta \right] + \dots \end{aligned} \quad (\text{A7})$$

But  $\bar{f}_3 = \bar{f}_{3x} = 0$ , so

$$\frac{dx}{d\tau} = \frac{\alpha}{T} \left[ \frac{1}{2} \bar{f}_2 \bar{f}_{3xx} x^2 + \bar{f}_2 \bar{f}_{3y}y + \bar{f}_2 \bar{f}_{3\beta}\beta \right] + \dots \quad (\text{A8})$$

To put Eq. (A8) into the canonical form of  $dx/d\tau$  in Eq. (15), we require

$$\frac{\alpha}{T} = \frac{2}{\bar{f}_2 \bar{f}_{3xx}} = \frac{-1}{\bar{f}_2 \bar{f}_{3y}}, \quad (\text{A9})$$

but

$$\begin{aligned} f_2 &= \frac{u}{1 + u^2} = \frac{\frac{x}{\alpha} + u_m}{1 + \left( \frac{x}{\alpha} + u_m \right)^2}, \\ f_3 &= \frac{\left[ a - \frac{x}{\alpha} - u_m \right] \left[ 1 + \left( \frac{x}{\alpha} + u_m \right)^2 \right] - \beta \left( \frac{x}{\alpha} + u_m \right)^2}{\frac{x}{\alpha} + u_m} \\ &\quad - \frac{y}{\rho} - w_m. \end{aligned} \quad (\text{A10})$$

Evaluating the derivatives gives

$$\begin{aligned} \bar{f}_2 &= \frac{u_m}{1 + u_m^2}, \\ \bar{f}_{3xx} &= \frac{2}{\alpha^2} \left( \frac{a - u_m^3}{u_m^3} \right), \\ \bar{f}_2 \bar{f}_{3xx} &= \frac{2}{\alpha^2} \left( \frac{a - u_m^3}{u_m^2(1 + u_m^2)} \right), \\ \bar{f}_{3y} &= -\frac{1}{\rho}, \\ \bar{f}_2 \bar{f}_{3y} &= -\frac{u_m}{1 + u_m^2} \left( \frac{1}{\rho} \right), \\ \bar{f}_{3\beta} &= -u_m. \end{aligned} \quad (\text{A11})$$

Combining Eqs. (A5), (A9), and (A11) to find the scale factors, we have

$$\begin{aligned}
 \frac{\alpha}{T} &= -\frac{1}{\bar{f}_2 \bar{f}_{3y}} = \frac{\rho(1+u_m^2)}{u_m}, \\
 \frac{\alpha}{T} &= \frac{2}{\bar{f}_2 \bar{f}_{3xx}} = \frac{\alpha^2 u_m^2 (1+u_m^2)}{a-u_m^3}, \\
 \frac{\rho(1+u_m^2)}{u_m} &= \frac{\alpha^2 u_m^2 (1+u_m^2)}{a-u_m^3}, \\
 \rho &= \frac{\alpha^2 u_m^3}{a-u_m^3}, \\
 \alpha T &= 5\rho = \frac{a-u_m^3}{u_m^2 (1+u_m^2)}, \\
 5 \left( \frac{\alpha^2 u_m^3}{a-u_m^3} \right) &= \frac{a-u_m^3}{u_m^2 (1+u_m^2)}, \\
 \alpha &= L = \frac{a-u_m^3}{[5u_m^5 (1+u_m^2)]^{1/2}}, \\
 \rho &= \left( \frac{a-u_m^3}{[5u_m^5 (1+u_m^2)]^{1/2}} \right)^2 \left( \frac{u_m^3}{a-u_m^3} \right) \\
 &= \frac{a-u_m^3}{5u_m^2 (1+u_m^2)}, \\
 T &= \frac{5\rho}{\alpha} = \frac{5(a-u_m^3)}{5u_m^2 (1+u_m^2)} \left( \frac{[5u_m^5 (1+u_m^2)]^{1/2}}{a-u_m^3} \right) \\
 &= \left( \frac{5u_m}{1+u_m^2} \right)^{1/2}. \tag{A12}
 \end{aligned}$$

Now for the higher order terms that give  $h_1$ ,  $h_2$ , and  $h_3$ , we can rewrite Eq. (A8) as

$$\begin{aligned}
 \frac{dx}{d\tau} &= \frac{\alpha}{T} \left[ \frac{1}{2} \bar{f}_2 \bar{f}_{3xx} x^2 + \frac{1}{6} (\bar{f}_2 \bar{f}_{3xxx} + 3\bar{f}_{2x} \bar{f}_{3xx} + 3\bar{f}_{2xx} \bar{f}_{3x} \right. \\
 &\quad \left. + 3\bar{f}_{2xxx} \bar{f}_3) x^3 + \bar{f}_2 \bar{f}_{3y} y + (\bar{f}_2 \bar{f}_{3xy} + \bar{f}_{2x} \bar{f}_{3y} + \bar{f}_{2xy} \bar{f}_3) xy \right. \\
 &\quad \left. + \frac{1}{2} \bar{f}_2 \bar{f}_{3yy} y^2 + (f_{2\beta} f_3 + f_2 f_{3\beta}) \beta \right] + \dots \\
 &= x^2 + \frac{\alpha}{6T} (\bar{f}_2 \bar{f}_{3xxx} + 3\bar{f}_{2x} \bar{f}_{3xx}) x^3 \\
 &\quad - y + \frac{\alpha}{T} \bar{f}_{2x} \bar{f}_{3y} xy + \frac{\alpha}{2T} \bar{f}_2 \bar{f}_{3yy} y^2 + \frac{\alpha}{T} \bar{f}_2 \bar{f}_{3\beta} \beta + \dots, \tag{A13}
 \end{aligned}$$

which allows us to identify

$$\begin{aligned}
 h_1 &= 1 - \frac{\alpha}{T} \bar{f}_{2x} \bar{f}_{3y} x - \frac{\alpha}{2T} \bar{f}_2 \bar{f}_{3yy} y, \\
 h_2 &= 1 + \frac{\alpha}{6T} (\bar{f}_2 \bar{f}_{3xxx} + 3\bar{f}_{2x} \bar{f}_{3xx}) x, \\
 h_3 &= \frac{\alpha}{T} \bar{f}_2 \bar{f}_{3\beta}, \tag{A14}
 \end{aligned}$$

$$\bar{f}_{2x} = -\frac{u_m^2 - 1}{\alpha (1+u_m^2)^2}, \tag{A15}$$

but  $\bar{f}_{3yy} = 0$ , so  $h_1$  is

$$\begin{aligned}
 h_1 &= 1 - \frac{\alpha}{T} \bar{f}_{2x} \bar{f}_{3y} x \\
 &= 1 - \frac{u_m^2 - 1}{\rho T (1+u_m^2)^2} x, \\
 \rho T &= \frac{a - u_m^3}{5u_m^2 (1+u_m^2)} \left( \frac{5u_m}{1+u_m^2} \right)^{1/2}, \\
 \frac{1}{\rho T} &= \frac{5u_m^2 (1+u_m^2) (1+u_m^2)^{1/2}}{(a-u_m^3)(5u_m)^{1/2}}, \\
 h_{1x} &= -\frac{u_m^2 - 1}{\rho T (1+u_m^2)^2} \\
 &= -\frac{5u_m^2 (u_m^2 - 1)}{(a-u_m^3)[5u_m (1+u_m^2)]^{1/2}}, \tag{A16}
 \end{aligned}$$

and

$$\begin{aligned}
 \bar{f}_{3xxx} &= -\frac{6a}{u_m^4 \alpha^3}, \\
 \bar{f}_2 \bar{f}_{3xxx} &= \frac{u_m}{1+u_m^2} \left( -\frac{6a}{u_m^4 \alpha^3} \right) = -\frac{6a}{u_m^3 \alpha^3 (1+u_m^2)}, \\
 3\bar{f}_{2x} \bar{f}_{3xx} &= -3 \frac{u_m^2 - 1}{\alpha (1+u_m^2)^2} \frac{2}{\alpha^2} \left( \frac{a - u_m^3}{u_m^3} \right) \\
 &= \frac{-6(u_m^2 - 1)(a - u_m^3)}{u_m^3 \alpha^3 (1+u_m^2)^2}, \\
 \alpha^2 T &= \frac{(a - u_m^3)^2}{5u_m^5 (1+u_m^2)} \left( \frac{5u_m}{1+u_m^2} \right)^{1/2}, \\
 \frac{1}{\alpha^2 T} &= \frac{5u_m^5 (1+u_m^2)^{3/2}}{(a - u_m^3)^2 (5u_m)^{1/2}}, \tag{A17}
 \end{aligned}$$

so

$$\begin{aligned}
 h_{2x} &= -\left( \frac{\alpha}{u_m^3 \alpha^3 T (1+u_m^2)} \right) \left[ a + \frac{(u_m^2 - 1)(a - u_m^3)}{(1+u_m^2)} \right] \\
 &= -\frac{5u_m^2 (2au_m^2 - u_m^5 + u_m^3)}{(a - u_m^3)^2 (5u_m)^{1/2} (1+u_m^2)^{1/2}}, \tag{A18}
 \end{aligned}$$

and

$$h_3 = -\frac{\alpha}{T} \left( \frac{u_m^2}{1+u_m^2} \right). \tag{A19}$$

## APPENDIX B: KRUPA-SZMOLYAN CANARD ANALYSIS OF THE COUPLED SYSTEM (SELF-DISINHIBITION)

The coupling term modifies only the second equation as shown in Eq. (B1). We maintain the notations in Eqs. (A1) and (A2) and introduce the subscript  $j$  for the self-disinhibition. From Krupa and Szmolyan [35], we want to put the autonomous part, Eq. (25), into canonical form of Eq. (15) by choosing  $\alpha_j$ ,  $\rho_j$ ,  $L_j$  and  $T_j$  so that in  $dx_j/d\tau$  in Eq. (15) there are no constants or  $x_j$  terms, and in Eq. (15) the constant terms

in  $h_{1j,2j,4j,5j}$  are 1. Thus, we obtain

$$\begin{aligned} \frac{dx_j}{d\tau} &= \frac{\alpha_j}{T_j} \left[ f_1 \left( \frac{x_j}{\alpha_j} + u_m, \beta \right) - \frac{y_j}{\rho_j} - w_m \right] f_2 \left( \frac{x_j}{\alpha_j} + u_m \right) \\ &\equiv \frac{\alpha_j}{T_j} f_3(x_j, y_j, \beta) f_2 \left( \frac{x_j}{\alpha_j} + u_m \right), \\ \frac{dy_j}{d\tau} &= \frac{\rho_j}{T_j} \beta \left( \frac{5x_j}{\alpha_j} - \frac{5\gamma_j}{L_j} - \frac{\beta D_v x_j}{\alpha_j} - \beta D_v u_m - \frac{D_v y_j}{\rho_j} \right. \\ &\quad \left. - D_v w_m \right). \end{aligned} \quad (\text{B1})$$

Comparing Eq. (B1) with Eq. (15) gives

$$\frac{\rho_j(5 - \beta D_v)}{\alpha_j T_j} = \frac{5\rho_j}{L_j T_j} = 1. \quad (\text{B2})$$

With the exception of  $h_6$ , the conditions and Eqs. (A6)–(A11) stay the same. The constants from the coupling for the self-disinhibition are then

$$\begin{aligned} \rho_j &= \frac{\alpha_j^2 u_m^3}{a - u_m^3}, \\ \alpha_j &= \left[ \frac{(a - u_m^3)^2}{u_m^5 (1 + u_m^2) (5 - \beta D_v)} \right]^{1/2}, \\ T_j &= \left[ \frac{u_m (5 - \beta D_v)}{1 + u_m^2} \right]^{1/2}, \\ L_j &= \left[ \frac{25(a - u_m^3)^2}{u_m^5 (1 + u_m^2) (5 - \beta D_v)^3} \right]^{1/2}. \end{aligned} \quad (\text{B3})$$

The higher order terms are

$$\begin{aligned} h_{1x_j} &= - \left[ \frac{u_m^3 (5 - \beta D_v) (u_m^2 - 1)^2}{(a - u_m^3)^2 (1 + u_m^2)} \right]^{1/2}, \\ h_{2x_j} &= - \left[ \frac{u_m^3 (5 - \beta D_v) (2a u_m^2 - u_m^5 + u_m^3)^2}{(1 + u_m^2) (a - u_m^3)^4} \right]^{1/2}, \\ h_{3j} &= - \frac{\alpha_j}{T_j} \left( \frac{u_m^2}{1 + u_m^2} \right), \\ h_{6j} &= \frac{\rho_j}{T_j} \bar{g}_{y_j} = \frac{D_v}{T_j}. \end{aligned} \quad (\text{B4})$$

From Krupa and Szmolyan [35],

$$\begin{aligned} a_{1j} &= \bar{h}_{3x_j} = \frac{d}{dx_j} (\bar{f}_2 \bar{f}_3 \beta) = \frac{d}{dx_j} \left[ - \frac{u_m^2}{(1 + u_m^2) \alpha_j} \right] \\ &= 0, \\ a_{2j} &= \bar{h}_{1x_j} = - \left[ \frac{u_m^3 (5 - \beta D_v) (u_m^2 - 1)^2}{(a - u_m^3)^2 (1 + u_m^2)} \right]^{1/2}, \\ a_{3j} &= \bar{h}_{2x_j} = - \left[ \frac{u_m^3 (5 - \beta D_v) (2a u_m^2 - u_m^5 + u_m^3)^2}{(1 + u_m^2) (a - u_m^3)^4} \right]^{1/2}, \\ a_{4j} &= \bar{h}_{4x_j} = 0, \\ a_{5j} &= h_{6j} = - \frac{D_v}{T_j} = - \left[ \frac{D_v^2 (1 + u_m^2)}{u_m (5 - \beta D_v)} \right]^{1/2}. \end{aligned} \quad (\text{B5})$$

Note that for the uncoupled case  $a_5 = 0$ , whereas for the diffusively coupled system  $a_{5j} \neq 0$ . This produces a slight change of the Hopf critical point as well as the canard critical point. The Hopf critical point is given by

$$\lambda_{jH}(\sqrt{\beta}) = - \left( \frac{a_{1j} + a_{5j}}{2L_{jH}} \right) \beta + \mathcal{O}(\beta^{3/2}), \quad (\text{B6})$$

and the canard critical point is given by

$$\lambda_{jc}(\sqrt{\beta}) = - \left( \frac{a_{1j} + a_{5j}}{2L_{jc}} + \frac{A_j}{8L_{jc}} \right) \beta + \mathcal{O}(\beta^{3/2}), \quad (\text{B7})$$

where

$$A_j = -a_{2j} + 3a_{3j} - 2a_{4j} - 2a_{5j}. \quad (\text{B8})$$

## APPENDIX C: STEADY STATES FOR SELF-DISINHIBITION AND CROSS-COUPING

To calculate the steady state of the SD scheme from Eq. (25), we set the second equation to zero and solve for  $w_i$  to get Eq. (C1)

$$w_i = \frac{-a + 5u_i - D_v u_i \beta}{D_v}. \quad (\text{C1})$$

We next substitute Eq. (C1) into the first equation of Eq. (25). At the steady state, we have

$$0 = \frac{aD_v + au_i - D_v u_i - 5u_i^2 + aD_v u_i^2 - D_v u_i^3}{D_v (1 + u_i^2)}. \quad (\text{C2})$$

We define the steady state as  $u_{i,\text{self}}^* = a/5 + \varsigma$ , which we substitute into Eq. (C2). We expand, drop the cubic term, and solve for  $\varsigma$ , choosing the root that approaches zero as  $D_v \rightarrow 0$ .

$$\varsigma = \frac{25a + 25D_v - 7a^2 D_v - \sqrt{625a^2 + 11250aD_v + 50a^3 D_v + 625D_v^2 - 1150a^2 D_v^2 + 17a^4 D_v^2}}{10(-25 + 2aD_v)}, \quad (\text{C3})$$

$$u_{i,\text{self}}^* \approx \frac{a}{5} + \frac{25a + 25D_v - 7a^2 D_v - \sqrt{625a^2 + 11250aD_v + 50a^3 D_v + 625D_v^2 - 1150a^2 D_v^2 + 17a^4 D_v^2}}{10(-25 + 2aD_v)}. \quad (\text{C4})$$

Equation (C4) represents the new steady state due to the self-disinhibition.

In the new variables, we have Eq. (C5) for the CC scheme

$$\begin{aligned}\frac{du_i}{dt} &= a - u_i - \frac{u_i(u_i\beta + w_i)}{1 + u_i^2}, \\ \frac{dw_i}{dt} &= \beta[5u_i - a + \beta D_v u_j + D_v w_j].\end{aligned}\quad (\text{C5})$$

At the steady state  $u_i = u_j$  and  $w_i = w_j$ . To calculate the steady state with the cross coupling we replace  $u_j$  by  $u_i$  and  $w_j$  by  $w_i$  and solve for  $w_{i,\text{cr}}^*$  as shown in Eq. (C6),

$$w_{i,\text{cr}}^* = \frac{a - (5 + D_v\beta)u_{i,\text{cr}}^*}{D_v}. \quad (\text{C6})$$

We substitute  $w_{i,\text{cr}}^*$  into the first equation of Eq. (27) and solve for the steady state value of  $u_{i,\text{cr}}^*$ :

$$\begin{aligned}0 &= (a - u_{i,\text{cr}}^*)(1 + u_{i,\text{cr}}^{*2}) - u_{i,\text{cr}}^* \left( \frac{a - 5u_{i,\text{cr}}^*}{D_v} \right), \\ 0 &= aD_v - (a + D_v)u_{i,\text{cr}}^* + (aD_v + 5)u_{i,\text{cr}}^{*2} - D_vu_{i,\text{cr}}^{*3}.\end{aligned}\quad (\text{C7})$$

We define the steady state as  $u_{i,\text{cr}}^* = a/5 - \varphi$ .

$$\begin{aligned}0 &= aD_v - (a + D_v)\left(\frac{a}{5} - \varphi\right) + (aD_v + 5)\left(\frac{a}{5} - \varphi\right)^2 - D_v\left(\frac{a}{5} - \varphi\right)^3, \\ 0 &= \frac{100aD_v + 4a^3D_v - (125a - 125D_v + 35a^2D_v)\varphi + (625 + 50aD_v)\varphi^2 + 125D_v\varphi^3}{125}.\end{aligned}\quad (\text{C8})$$

Dropping the cubic term in  $\varphi$  in Eq. (C8) yields and solving the quadratic for  $\varphi$  gives

$$\varphi = \frac{25a - 25D_v + 7a^2D_v - \sqrt{625a^2 - 11250aD_v - 50a^3D_v + 625D_v^2 - 1150a^2D_v^2 + 17a^4D_v^2}}{10(25 + 2aD_v)}. \quad (\text{C9})$$

The steady state of  $u$  shifts by

$$u_{i,\text{cr}}^* \approx \frac{a}{5} - \frac{25a - 25D_v + 7a^2D_v - \sqrt{625a^2 - 11250aD_v - 50a^3D_v + 625D_v^2 - 1150a^2D_v^2 + 17a^4D_v^2}}{10(25 + 2aD_v)}. \quad (\text{C10})$$

Since  $a \gg D_v$ , the steady states given by Eqs. (C4) and (C10) are shifted by roughly the same (small) amount but in opposite directions, as shown in Fig. 8.

---

[1] M. Bennett, M. F. Schatz, H. Rockwood, and K. Wiesenfeld, Huygens's clocks, *Proc. R. Soc. A* **458**, 563 (2002).

[2] T. Pereira, M. S. Baptista, and J. Kurths, Multi-time-scale synchronization and information processing in bursting neuron networks, *Eur. Phys. J.: Spec. Top.* **146**, 155 (2007).

[3] Y. Wu, J. Xu, and W. Jin, Synchronous behaviors of two coupled neurons, in *Advances in Neural Networks (ISNN 2005)*, edited by J. Wang, X. Liao, and Z. Yi (Springer, Berlin/Heidelberg, 2005), pp. 302–307.

[4] R. C. Elson, A. I. Selverston, R. Huerta, N. F. Rulkov, M. I. Rabinovich, and H. D. I. Abarbanel, Synchronous Behavior of Two Coupled Biological Neurons, *Phys. Rev. Lett.* **81**, 5692 (1998).

[5] E. Izhikevich, Synchronization of elliptic bursters, *SIAM Rev.* **43**, 315 (2001).

[6] M. Dhamala, V. K. Jirsa, and M. Ding, Transitions to Synchrony in Coupled Bursting Neurons, *Phys. Rev. Lett.* **92**, 028101 (2004).

[7] I. Belykh, E. de Lange, and M. Hasler, Synchronization of Bursting Neurons: What Matters in the Network Topology, *Phys. Rev. Lett.* **94**, 188101 (2005).

[8] Y. Wang and J. E. Rubin, Timescales and mechanisms of sigh-like bursting and spiking in models of rhythmic respiratory neurons, *J. Math. Neurosci.* **7**, 3 (2017).

[9] E. Köksal Ersöz, A. Vidal, and F. Clément, Coupled multiple timescale dynamics in populations of endocrine neurons: Pulsatile and surge patterns of GnRH secretion, *SIAM J. Appl. Dyn. Syst.* **17**, 1052 (2018).

[10] E. Benoit, J. Louis Callot, F. Diener, and M. Diener, Chasse au canard, *Collectanea Mathematica* **32**, 37 (1981).

[11] M. Brøns and K. Bar-Eli, Canard explosion and excitation in a model of the Belousov-Zhabotinskii reaction, *J. Phys. Chem.* **95**, 8706 (1991).

[12] M. Desroches and M. R. Jeffrey, Canards and curvature: The “smallness of  $\varepsilon$ ” in slow-fast dynamics, *Proc. R. Soc. A* **467**, 2404 (2011).

[13] M. Desroches, B. Krauskopf, and H. M. Osinga, Mixed-mode oscillations and slow manifolds in the self-coupled Fitzhugh-Nagumo system, *Chaos* **18**, 015107 (2008).

[14] M. Desroches, B. Krauskopf, and H. Osinga, The geometry of slow manifolds near a folded node, *SIAM J. Appl. Dyn. Syst.* **7**, 1131 (2008).

[15] M. Desroches, B. Krauskopf, and H. M. Osinga, The geometry of mixed-mode oscillations in the Olsen model for the peroxidase-oxidase reaction, *Disc. Cont. Dyn. Syst.* **2**, 807 (2009).

[16] M. Desroches, B. Krauskopf, and H. M. Osinga, Numerical continuation of canard orbits in slow-fast dynamical systems, *Nonlinearity* **23**, 739 (2010).

[17] M. Desroches, J. Guckenheimer, B. Krauskopf, C. Kuehn, H. Osinga, and M. Wechselberger, Mixed-mode oscillations with multiple timescales, *SIAM Rev.* **54**, 211 (2012).

[18] M. Desroches, T. J. Kaper, and M. Krupa, Mixed-mode bursting oscillations: Dynamics created by a slow passage through spike-adding canard explosion in a square-wave burster, *Chaos* **23**, 046106 (2013).

[19] H. G. Rotstein, N. Kopell, A. M. Zhabotinsky, and I. R. Epstein, A canard mechanism for localization in systems of globally coupled oscillators, *SIAM J. Appl. Math.* **63**, 1998 (2003).

[20] H. G. Rotstein, N. Kopell, A. M. Zhabotinsky, and I. R. Epstein, Canard phenomenon and localization of oscillations in the Belousov-Zhabotinsky reaction with global feedback, *J. Chem. Phys.* **119**, 8824 (2003).

[21] D. M. Abrams and S. H. Strogatz, Chimera States for Coupled Oscillators, *Phys. Rev. Lett.* **93**, 174102 (2004).

[22] M. J. Panaggio and D. M. Abrams, Chimera states: Coexistence of coherence and incoherence in networks of coupled oscillators, *Nonlinearity* **28**, R67 (2015).

[23] D. M. Abrams, R. Mirolo, S. H. Strogatz, and D. A. Wiley, Solvable Model for Chimera States of Coupled Oscillators, *Phys. Rev. Lett.* **101**, 084103 (2008).

[24] L. Schmidt, K. Schönleber, K. Krischer, and V. Garcia-Morales, Coexistence of synchrony and incoherence in oscillatory media under nonlinear global coupling, *Chaos* **24**, 013102 (2014).

[25] E. A. Martens, S. Thutupalli, A. Fourrière, and O. Hallatschek, Chimera states in mechanical oscillator networks, *Proc. Nat. Acad. Sci. U.S.A.* **110**, 10563 (2013).

[26] I. Omelchenko, Y. Maistrenko, P. Hövel, and E. Schöll, Loss of Coherence in Dynamical Networks: Spatial Chaos and Chimera States, *Phys. Rev. Lett.* **106**, 234102 (2011).

[27] B. K. Bera, S. Majhi, D. Ghosh, and M. Perc, Chimera states: Effects of different coupling topologies, *Europhys. Lett.* **118**, 10001 (2017).

[28] S. Majhi, B. K. Bera, D. Ghosh, and M. Perc, Chimera states in neuronal networks: A review, *Phys. Life Revs.* **28**, 100 (2019).

[29] J. Wojewoda, K. Czolczynski, Y. Maistrenko, and T. Kapitaniak, The smallest chimera state for coupled pendula, *Sci. Rep.* **6**, 34329 (2016).

[30] Y. Maistrenko, S. Brezetsky, P. Jaros, R. Levchenko, and T. Kapitaniak, Smallest chimera states, *Phys. Rev. E* **95**, 010203(R) (2017).

[31] N. M. Awal, D. Bullara, and I. R. Epstein, The smallest chimera: Periodicity and chaos in a pair of coupled chemical oscillators, *Chaos* **29**, 013131 (2019).

[32] I. Lengyel, G. Rábai, and I. R. Epstein, Experimental and modeling study of oscillations in the chlorine dioxide-iodide-malonic acid reaction, *J. Am. Chem. Soc.* **112**, 9104 (1990).

[33] I. Lengyel and I. R. Epstein, Modeling of turing structures in the chlorite-iodide-malonic acid-starch reaction system, *Science* **251**, 650 (1991).

[34] W. M. Ni and M. Tang, Turing patterns in the Lengyel-Epstein system for the CIMA reaction, *Trans. Am. Math. Soc.* **357**, 3953 (2005).

[35] M. Krupa and P. Szmolyan, Extending geometric singular perturbation theory to nonhyperbolic points—Fold and canard points in two dimensions, *SIAM J. Math. Anal.* **33**, 286 (2001).

[36] See Supplemental Material at <http://link.aps.org/supplemental/10.1103/PhysRevE.101.042222> for list of tables of the different coupling schemes used to generate the bifurcation diagrams and supplemental videos of the “leapfrogging” and “three-way” MMOs.

[37] H. G. Rotstein and R. Kuske, Localized and asynchronous patterns via canards in coupled calcium oscillators, *Physica D* **215**, 46 (2006).